GSA DATA REPOSITORY 2016216

# Appendix DR1. Description of sedimentological datasets, Table DR1, Figures DR1-DR20

## Vigorous deep-sea currents cause global anomaly in sediment accumulation in the Southern Ocean

Adriana Dutkiewicz*, R. Dietmar Müller, Andrew McC. Hogg, and Paul Spence

*corresponding author: adriana.dutkiewicz@sydney.edu.au

### DATASETS

#### Holocene sediment ages

Our unconformity-conformity dataset was supplemented by dated sediment cores from the Southern Ocean not found in the Chase and Burckle (2015) dataset. The sediment cores are: PS2090-1 and PS1654-2 (Bianchi and Gersonde, 2004a; Bianchi and Gersonde, 2004b; Bianchi and Gersonde, 2004c), MD07-3076 (Skinner et al., 2010a, b), RC11-83 (Charles and Fairbanks, 1992a; Charles and Fairbanks, 1992b), MD84-551, MD84-527 and MD73-025 (Labracherie et al., 1989a, b; Labracherie et al., 1989c), MD88-770 (Labeyrie et al., 1996a, b), MR0806-PC09, MD07-3128 and 202-1233 (Lamy et al., 2015a, b, c, d), PS2038-2, PS1821-6 and PS1575-1 (Bonn et al., 1998a, b, c, d), OSO0910_KC04, OSO0910_KC09, OSO0910_KC10, OSO0910_KC15, OSO0910_KC19, OSO0910_KC23 and DF81_PC07 (Kirshner et al., 2012a, b), RC12-225 and MD84-529 (Howard and Prell, 1994a, b; Howard and Prell, 1994c), GOMEA-06, GOMEA-14, GOMEA-15 and GOMEA-16 (Gozhik et al., 1991a, b), PS2082 and PS1506-1 (Mackensen et al., 1994a, b, c), PS75/083-1, PS75/079-2, PS75/076-2, PS75/074-3, PS75/059-2 and PS75/056-1 (Lamy et al., 2014a, b, c, d, e, f, g), TSP-2MC, TSP-3MC and TSP-2PC (Murayama et al., 2000a, b), TTN057-13-PC4 (Shemesh et al., 2002a, b), RC13-229, MD88-769 and MD80-304 (Rosenthal et al., 1995a, b, c, d), KC073 (Allen et al., 2005a, b), DF79.012-GB, DF79.009-GB, Core302 and 119-740A (Domack et al., 1991a, b, c, d, e), MD03-2597, NBP01-01-KC17B and NBP01-01-JPC17B (Maddison et al., 2012a, b), PS1380-3 (Grobe and Mackensen, 1992a, b), PS1786-1, PS2606-6 and PS58/271-1 (Jacot Des Combes et al., 2008a, b).

We carefully reviewed all *Eltanin* sites from Watkins and Kennett (1972) that had been re-analyzed by Osborn et al. (1983) and in rare instances of discrepancies in polarity assignment we use the Osborn et al. (1983) ages as the polarity measurements were made using a more sensitive magnetometer and with improved biostratigraphic control. There is very good agreement between the Bruhnes-age assignment of the majority of *Eltanin* core tops dated by magnetostratigraphy and by subsequent more highly-resolved methods (Chase and Burckle, 2015). Rare exceptions include *Eltanin* cores E14-5 and E20-10 which were very well-dated by Chase et al. (2003) and contradicted the earlier results of Goodell and Watkins (1968); in these cases the Chase et al. (2003) dates are used.

## Focusing factors

Focusing factors were calculated using the simplified equation from Dezileau et al. (2000):

$$\boldsymbol{\psi} = \frac{\boldsymbol{F}}{\boldsymbol{F_{vertical}}}$$

where $F_{\text{vertical}}$ is the sediment rain rate (g/cm$^2$/ka) for an age-dated stratigraphic section; $F$ is the accumulation rate (g/cm$^2$/ka); ψ is the focusing factor (Dezileau et al., 2000; Francois et al., 1993; Francois et al., 2004; Suman and Bacon, 1989). The accumulation rates were calculated from linear sedimentation segments from wells in which the age model is derived from $^{14}$C dating, oxygen isotopes or a combination of oxygen isotopes and biostratigraphy and/or $^{14}$C dating (see Table DR1 for list of cores) and dry bulk density for a given sample. Dry bulk densities were calculated using known $CaCO_3$ content and the best-fit second-order polynomial relationship of Froelich et al. (1991):

$$\boldsymbol{B_D} = \left(\mathbf{5.313 \times 10^{-5}}\right) \times (\boldsymbol{CaCO_3})^{\mathbf{2}} + (\mathbf{9.346 \times 10^{-4}}) \times (\boldsymbol{CaCO_3}) + \mathbf{0.3367}$$

where $B_D$ is dry bulk density (g/cm$^3$). In the absence of $CaCO_3$ measurements for a small number of cores (see Table DR1), a mean dry bulk density of 0.4 g cm$^{-3}$ for siliceous sediment (Geibert et al., 2005) was used. All values of $F_{\text{vertical}}$ (i.e., $^{230}$Th-normalized sediment flux) were obtained from references cited in Table DR1. As most of the cores contain multiple measurements of $CaCO_3$ and corresponding $^{230}$Th-normalized sediment flux over the interval of interest, our focusing factors are averages over those intervals.

Errors for focusing factors are very difficult to estimate and are rarely reported. For example, values given in Dezileau et al. (2000) and Frank et al. (1999) are given without errors although Frank et al. (1999) suggests that ψ is meaningful if it is significantly smaller (i.e., < 50%) or greater (i.e., > 50%) than 1. For core MD88-773, Yu (1994) gives an error range of ± 0.3 for focusing factors of 9.5 and 3.2. Despite uncertainties, Francois et al. (2004) argue that focusing factors are good proxies for sediment focusing.

**Table DR1.** Location, water depth, sedimentation rates and focusing factors (average over the interval of interest) for cores from the Southern Ocean. Sedimentation rates and focusing factors are for the Holocene (defined as 0-13 ka by Delzileau et al. (2003) and applied here for comparability reasons) except in the case of Yu (1994) data where the values represent the period 0-18 ka. Values in bold are from cited references, all other values were calculated using age models and $^{230}$Th-normalized mass fluxes from cited references. *$CaCO_3$ measurement not available. See supplementary text for detail.

| Core | Lat. | Long. | Water Depth (m) | Sedimentation rate (cm/kyr) | Focusing factor | Reference |
|---|---|---|---|---|---|---|
| E11-3 | -56.90 | -115.24 | 4023 | 2 | 2.5 | Bradtmiller et al. (2009) |
| E11-4* | -57.83 | -115.22 | 4774 | 1.4 | 1.3 | Bradtmiller et al. (2009) |
| E11-7* | -60.92 | -114.78 | 5029 | 2 | 1.2 | Bradtmiller et al. (2009) |
| E11-12* | -65.87 | -115.08 | 4718 | 1 | 0.7 | Bradtmiller et al. (2009) |
| E14-16 | -58.99 | -125.03 | 4499 | 10 | 5.8 | Bradtmiller et al. (2009) |
| E14-17 | -57.83 | -124.95 | 3904 | 6.5 | 5.3 | Bradtmiller et al. (2009) |
| E15-4 | -59.02 | -99.76 | 4910 | 5 | 5.8 | Bradtmiller et al. (2009) |
| E15-5 | -58.02 | -99.98 | 4307 | 2.5 | 3.7 | Bradtmiller et al. (2009) |
| E15-6 | -59.97 | -101.32 | 4517 | 2 | 1.8 | Bradtmiller et al. (2009) |
| E15-12 | -58.68 | -108.80 | 4572 | 1 | 0.6 | Bradtmiller et al. (2009) |
| E15-28 | -56.02 | -149.82 | 3328 | 2 | 1 | Bradtmiller et al. (2009) |
| E17-7 | -61.08 | -134.35 | 4435 | 2 | 0.7 | Bradtmiller et al. (2009) |
| E19-6* | -61.93 | -107.96 | 5064 | 1 | 0.6 | Bradtmiller et al. (2009) |
| E19-7 | -62.16 | -109.09 | 5051 | 2.5 | 1 | Bradtmiller et al. (2009) |
| E20-13 | -55.00 | -104.95 | 3895 | 1 | 1.6 | Bradtmiller et al. (2009) |
| E21-20* | -60.25 | -120.17 | 4701 | 3.3 | 1.6 | Bradtmiller et al. (2009) |
| E23-14 | -63.82 | -108.85 | 4957 | 1 | 0.5 | Bradtmiller et al. (2009) |
| E23-17* | -60.22 | -114.63 | 5026 | 2 | 0.9 | Bradtmiller et al. (2009) |
| E23-18 | -58.98 | -115.00 | 5272 | 2 | 0.9 | Bradtmiller et al. (2009) |
| E25-16 | -56.15 | -156.22 | 3621 | 2.5 | 1.5 | Bradtmiller et al. (2009) |
| E27-23 | -59.62 | 155.24 | 3182 | 43.5 | 17.8 | Bradtmiller et al. (2009) |
| E33-19 | -59.86 | -119.66 | 4389 | 2.5 | 1.2 | Bradtmiller et al. (2009) |
| E36-36 | -60.39 | 157.53 | 2816 | 3.8 | 1 | Bradtmiller et al. (2009) |
| RC8-71 | -58.05 | 155.73 | 3224 | 2.6 | 1.6 | Bradtmiller et al. (2009) |
| VM16-115 | -55.68 | 141.28 | 3147 | 2.4 | 0.8 | Bradtmiller et al. (2009) |
| VM16-121 | -50.67 | 164.38 | 3614 | 5.1 | 1.5 | Bradtmiller et al. (2009) |
| VM17-88* | -57.03 | -74.48 | 4063 | 1.3 | 0.2 | Bradtmiller et al. (2009) |
| VM17-90* | -60.13 | -74.93 | 4568 | 0.6 | 0.4 | Bradtmiller et al. (2009) |
| VM18-73* | -61.53 | -73.28 | 4568 | 1.8 | 1.4 | Bradtmiller et al. (2009) |
| VM18-93 | -59.48 | -64.78 | 3834 | 1.6 | 0.9 | Bradtmiller et al. (2009) |
| MD 94-102 | -43.50 | 79.80 | 3205 | 5.9 | **3.3** | Dezileau et al. (2000) |
| MD 94-104 | -46.50 | 88.10 | 3460 | 12.5 | **8.8** | Dezileau et al. (2000) |
| MD 88-769 | -46.10 | 90.10 | 3420 | 4.1 | **2.6** | Dezileau et al. (2000) |
| MD 88-770 | -46.00 | 96.50 | 3290 | 6.8 | **3.6** | Dezileau et al. (2000) |
| MD 84-527 | -43.50 | 51.20 | 3269 | **27** | **10** | Dezileau et al. (2000); Francois et al. (1993) |
| MD 88-773 | -52.55 | 109.50 | 2460 | 27.4 | **9.5** | Yu (1994) |
| MD 84-552 | -54.90 | 73.80 | 1780 | 22.1 | **5** | Dezileau et al. (2000) |
| PS1772-8 | -55.46 | 1.16 | 4137 | 1.3 | **0.6** | Frank et al. (1999); Frank (2002b) |

| Core | Lat. | Long. | Water Depth (m) | Sedimentation rate (cm/kyr) | Focusing factor | Data Reference |
|---|---|---|---|---|---|---|
| PS1768-8 | -52.59 | 4.48 | 3299 | 13.75 | **4.6** | Frank et al. (1999); Mackensen (1996) |
| PS1756-5 | -48.90 | 6.71 | 3828 | 7.5 | **0.7** | Frank et al. (1999); Frank and Mackensen (2002a) |
| PS1754-1 | -46.77 | 7.61 | 2519 | 1.7 | **1.2** | Frank et al. (1999); Frank (2002a) |
| PS2082-1 | -43.22 | 11.74 | 4610 | 2.6 | **2** | Frank et al. (1999); Frank and Mackensen (2002b) |
| PS2498-1 | -44.15 | -14.23 | 3783 | 6.3 | **5.7** | Frank et al. (1999); Mackensen et al. (2001a) |
| PS2499-5 | -46.51 | -15.33 | 3175 | 2.9 | **2.2** | Frank et al. (1999); Mackensen et al. (2001b) |
| E49-29 | -57.10 | 94.96 | 4237 | 2.4 | 0.7 | Yu (1994) and references therein |
| E48-3 | -41.02 | 100.01 | 3930 | 1.4 | 2.1 | Yu (1994) and references therein |
| E50-8 | -50.93 | 104.91 | 3227 | 9.4 | 1.5 | Yu (1994) and references therein |
| E45-27 | -43.31 | 105.55 | 3776 | 1.6 | 1.3 | Yu (1994) and references therein |
| E45-29 | -44.88 | 106.52 | 3863 | 2.6 | 3.3 | Yu (1994) and references therein |
| E49-6 | -51.01 | 109.99 | 3326 | 2.3 | 1.1 | Yu (1994) and references therein |
| E49-8 | -55.07 | 110.02 | 3693 | 5.9 | 1.3 | Yu (1994) and references therein |
| E45-64 | -52.48 | 114.09 | 3823 | 8.1 | 2.7 | Yu (1994) and references therein |
| E45-63 | -53.44 | 114.26 | 3915 | 8.2 | 2.6 | Yu (1994) and references therein |
| E45-79 | -45.06 | 114.37 | 4079 | 1.9 | 2.6 | Yu (1994) and references therein |
| E45-74 | -47.55 | 114.44 | 3744 | 1.4 | 1.5 | Yu (1994) and references therein |
| E45-71 | -48.03 | 114.49 | 3658 | 2.1 | 2.2 | Yu (1994) and references therein |
| E49-8 | -55.07 | 110.02 | 3693 | 5.9 | 1.3 | Yu (1994) and references therein |
| E48-13 | -28.31 | 93.30 | 3380 | 5.9 | 8.8 | Yu (1994) and references therein |
| E48-11 | -29.40 | 97.32 | 3462 | 1.7 | 1.0 | Yu (1994) and references therein |
| E48-27 | -38.33 | 79.54 | 3285 | 2.9 | 2.9 | Yu (1994) and references therein |
| E48-22 | -39.54 | 85.25 | 3378 | 3.7 | 3.2 | Yu (1994) and references therein |
| E50-13 | -60.00 | 105.00 | 4209 | 2.1 | 0.3 | Yu (1994) and references therein |
| E50-17 | -62.00 | 120.03 | 4081 | 5.1 | 1.0 | Yu (1994) and references therein |

## $CaCO_3$ and $bSiO_2$ content of surface sediments

Our maps of $CaCO_3$ and $bSiO_2$ percentages in surface sediments are based on combined datasets from Chase and Burckle (2015), Archer (1996), Archer (1999) and Bohrmann (1999).

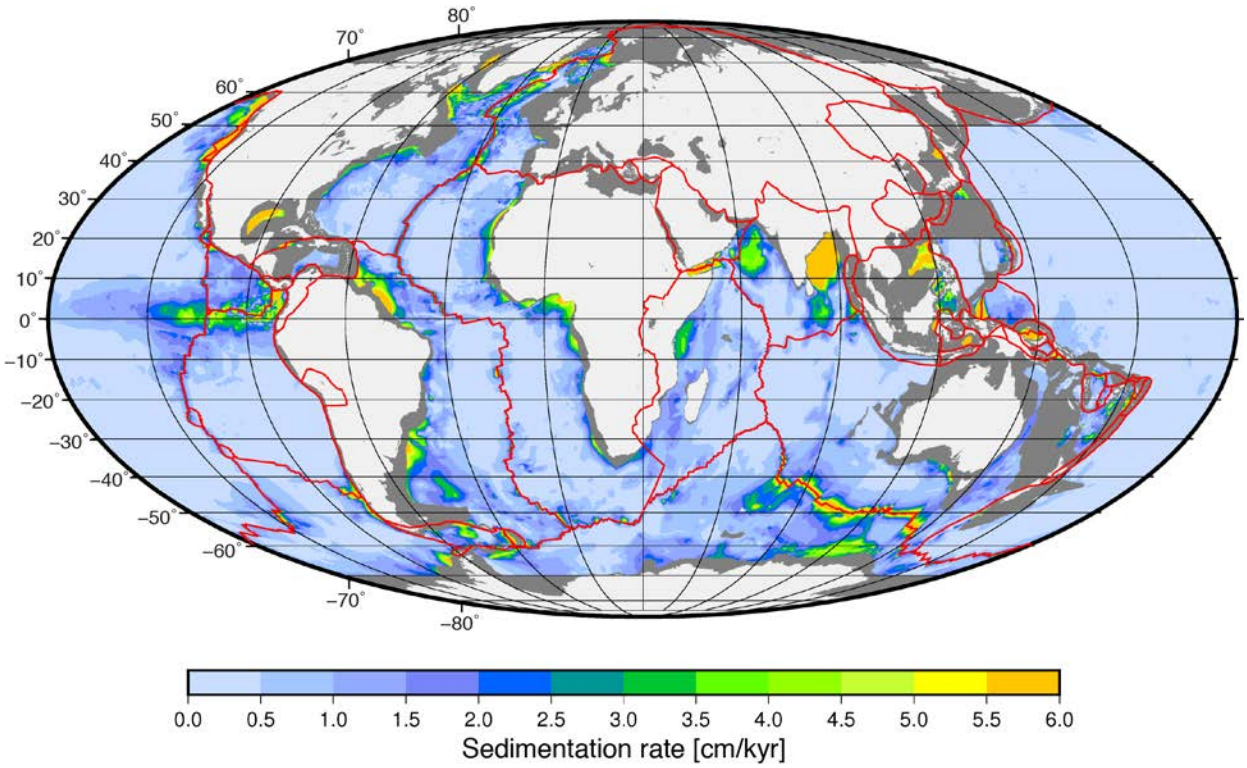


**Figure DR1.** Long-term average sedimentation rates in the world's ocean calculated using the global sediment thickness dataset of Whittaker et al. (2013) incorporating the dataset of Divins (2004), which represent minimum sediment thickness estimates, and the age grid of Müller et al. (2016). Red lines indicate plate boundaries. See also Figs. DR2 and DR3. Mollweide projection.

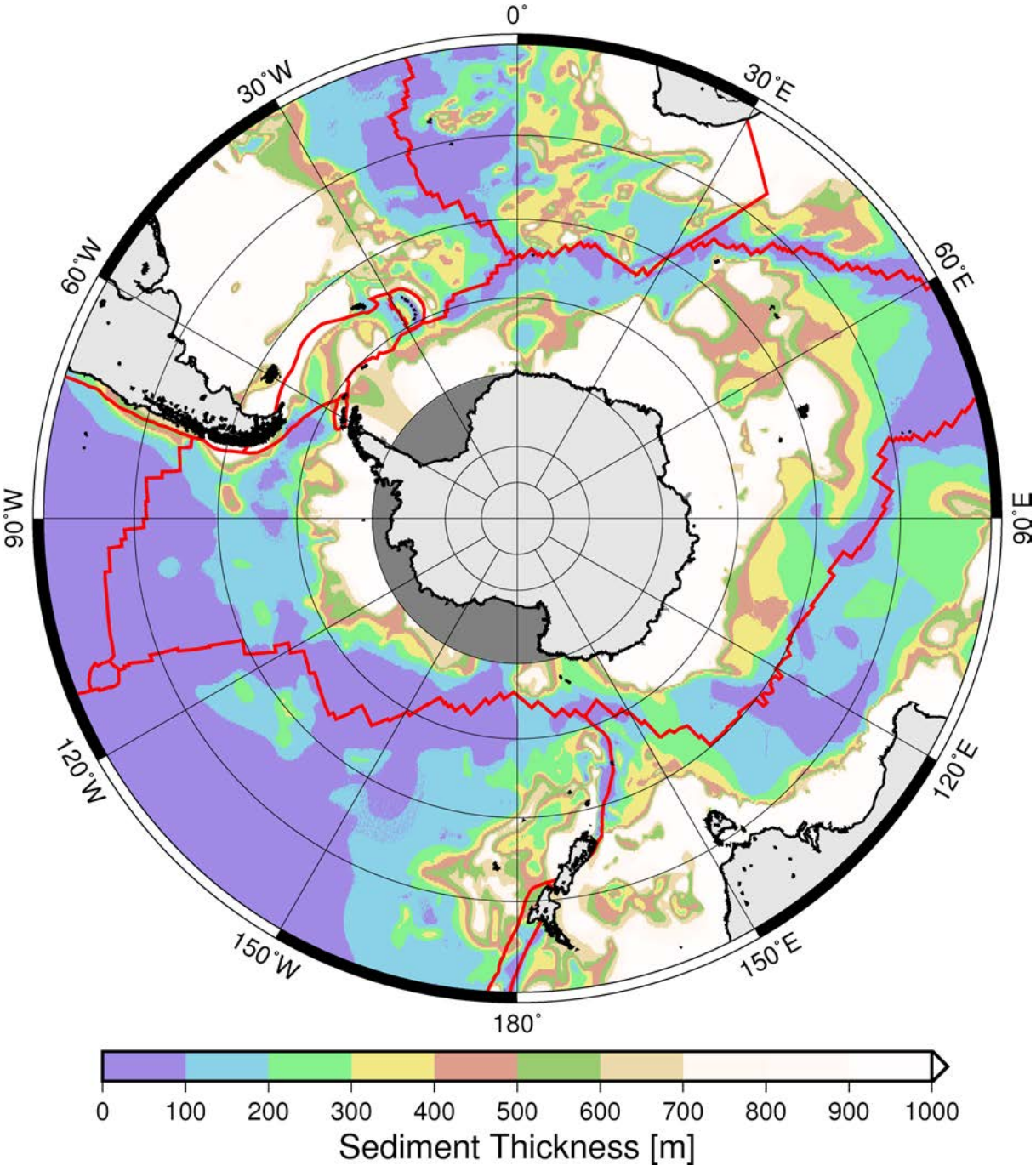


**Figure DR2.** Minimum sediment thickness estimates based on the global sediment thickness dataset of Whittaker et al. (2013) incorporating the dataset of Divins (2004). Red lines indicate plate boundaries. Stereographic projection.

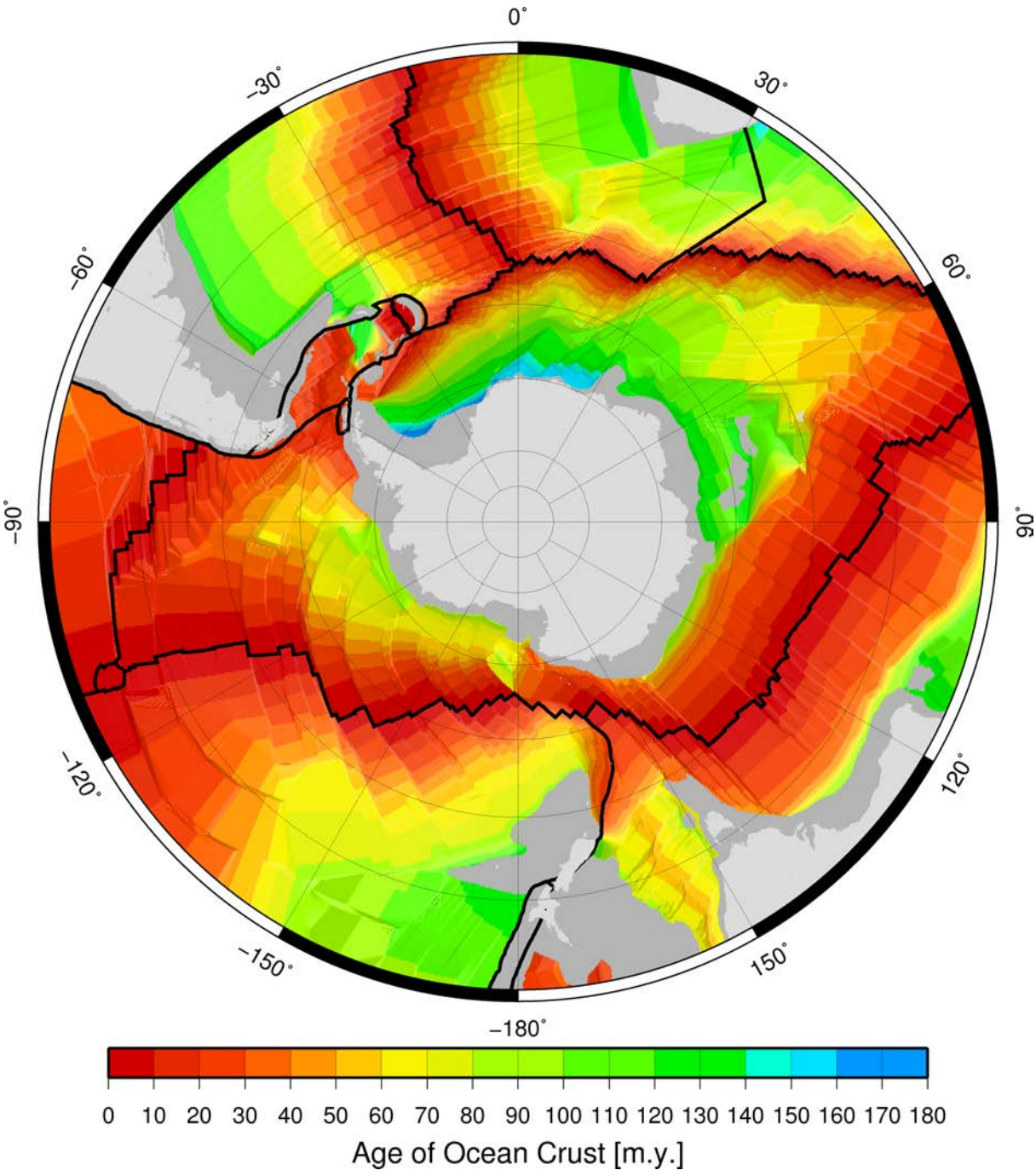


**Figure DR3.** Age of ocean crust from Müller et al. (2016). Black lines indicate plate boundaries with subaerial portions of continents shown in light grey and submerged continental crust in medium grey. Stereographic projection.

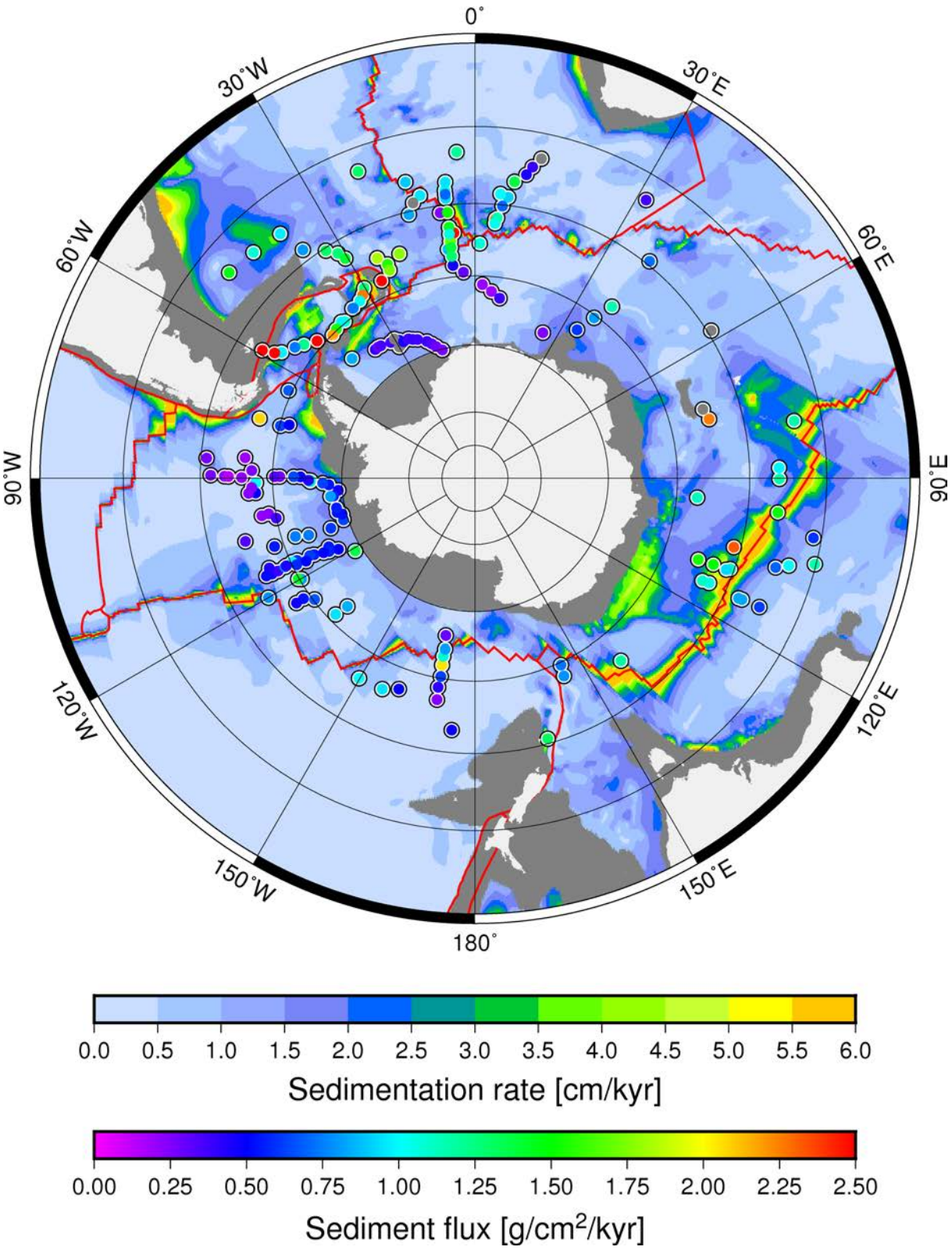


**Figure DR4.** Th-normalized sediment flux (circles) from Chase and Burckle, (2015) over long-term average sedimentation rates as in Figure DR1. Red lines indicate plate boundaries. Stereographic projection.

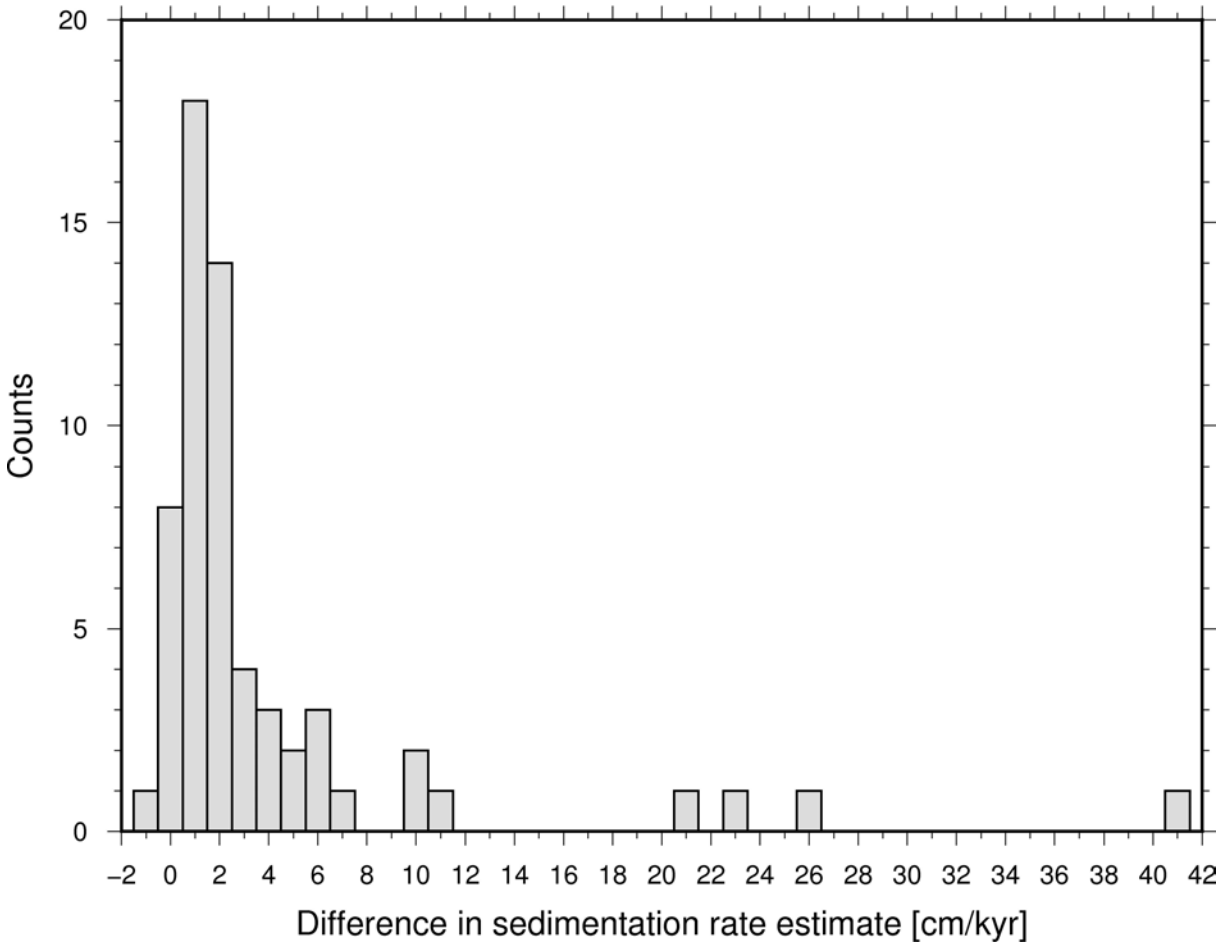


**Figure DR5.** Difference in sedimentation rate calculated using long-term average sedimentation rate (see Fig. DR1 caption for detail) minus Holocene sedimentation rate calculated using age-models for cores listed in Table DR1. The median difference is 1.7 cm/kyr, with a mean difference of 4 cm/kyr reflecting the influence of outliers due to high Holocene sedimentation rates at some locations (see Fig. 1A).

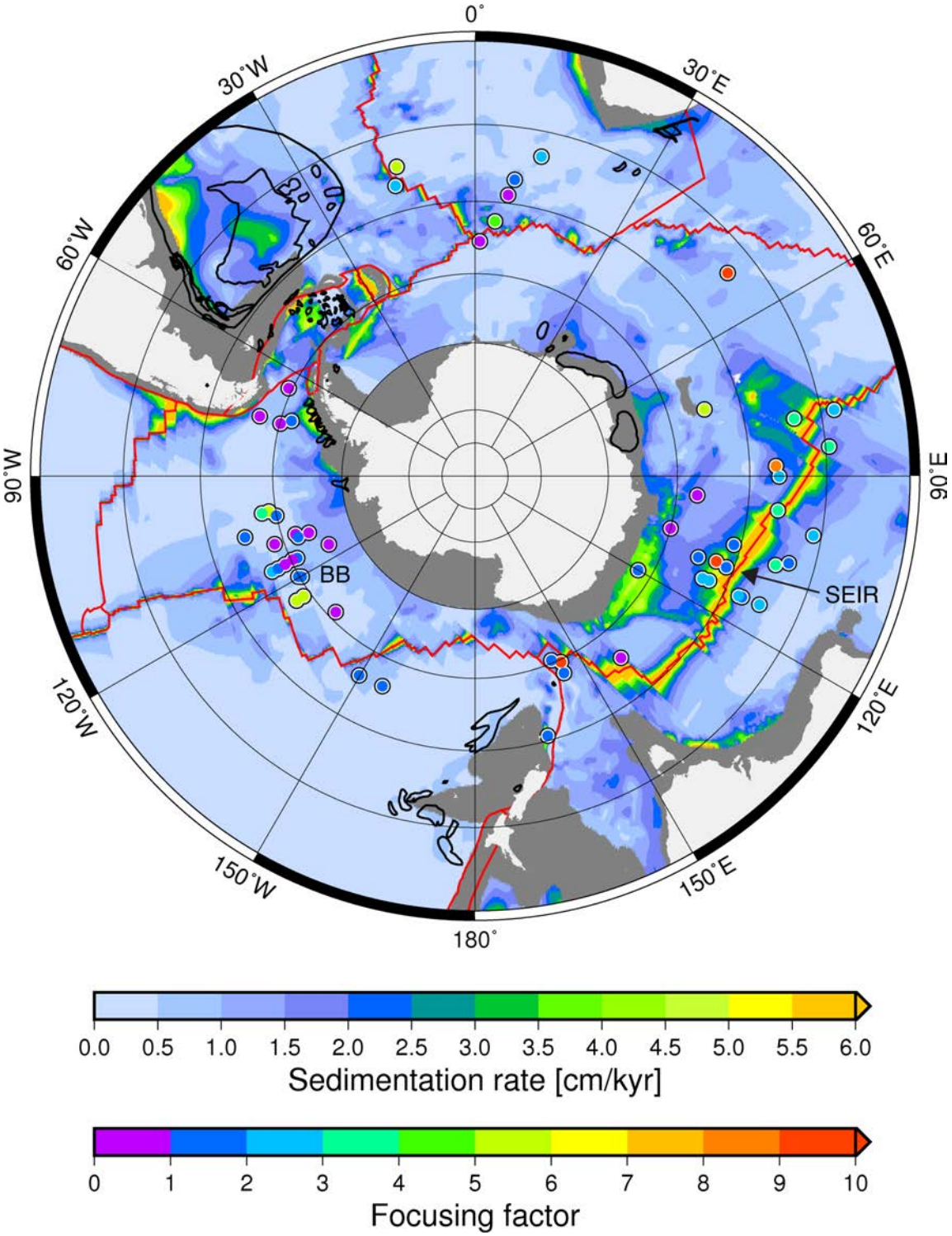


**Figure DR6.** Focusing factors (colored circles) overlying long-term sedimentation rates in the Southern Ocean. Focusing factors along the Southeast Indian Ridge (SEIR) are consistently and significantly greater than 1. In the Bellingshausen Basin (BB) the majority of focusing factors range between 0.5 and 1.5 with only 3 values > 5. Data in other parts of the Southern Ocean are relatively sparse. Black outlines indicate known large contourite deposits from Rebesco et al. (2014) available at http://www.marineregions.org/. Red lines denote plate boundaries. Stereographic projection.

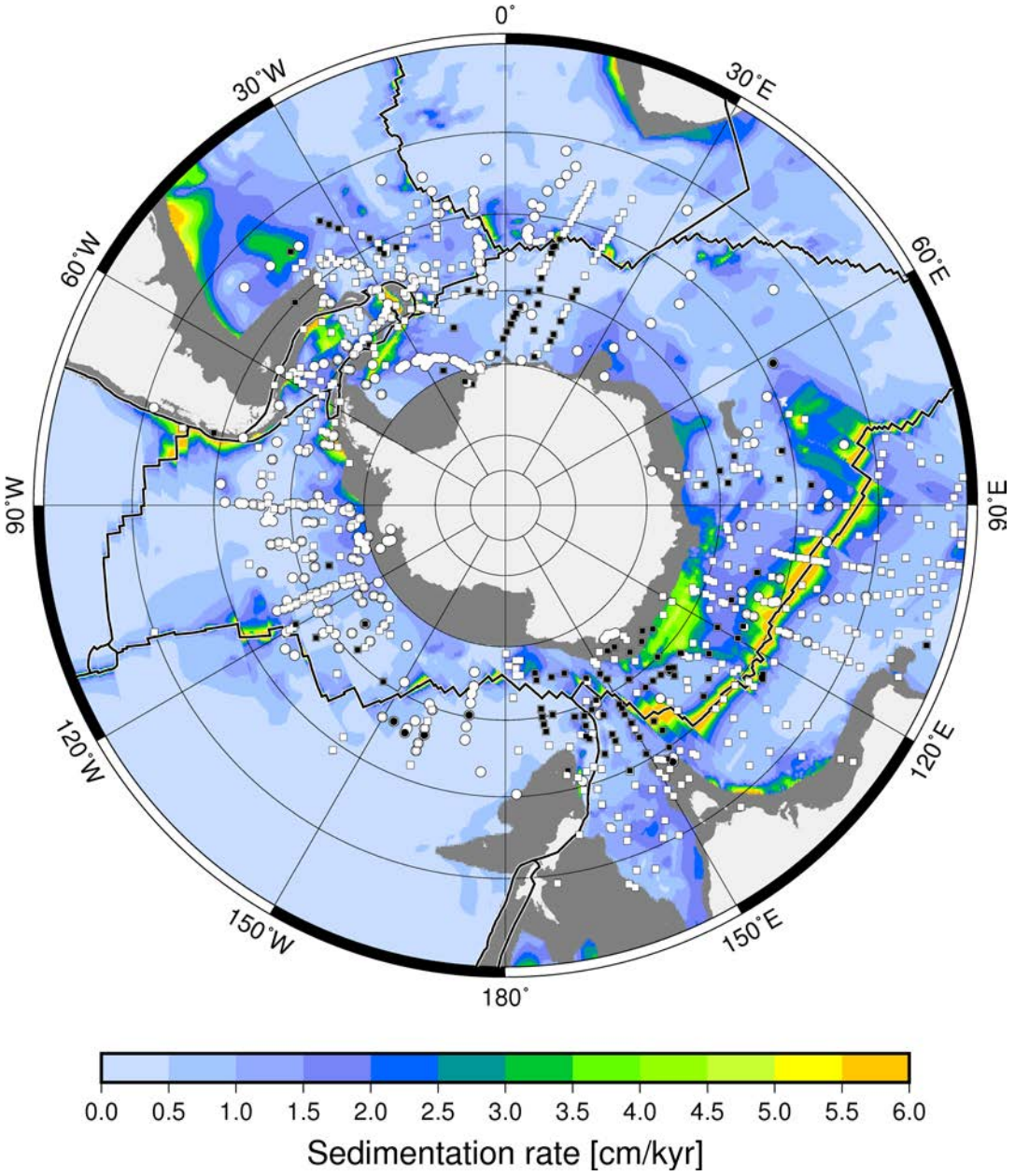


**Figure DR7.** Long-term average sedimentation rates overlain by conformities (white squares and white circles) and unconformities (black squares and black circles) in surface sediment of Bruhnes age. Squares represent magnetostratigraphic data from Watkins and Kennett (1972), Kennett and Watkins (1976), Osborn et al. (1983) and Ledbetter and Ciesielski (1986). Circles represent Holocene sediment dated by $^{14}C$ and undisturbed surface sediment from the Chase et al. (2015) compilation as well as additional data from various sources (see section on datasets in this Data Repository). Black lines denote plate boundaries. Stereographic projection.

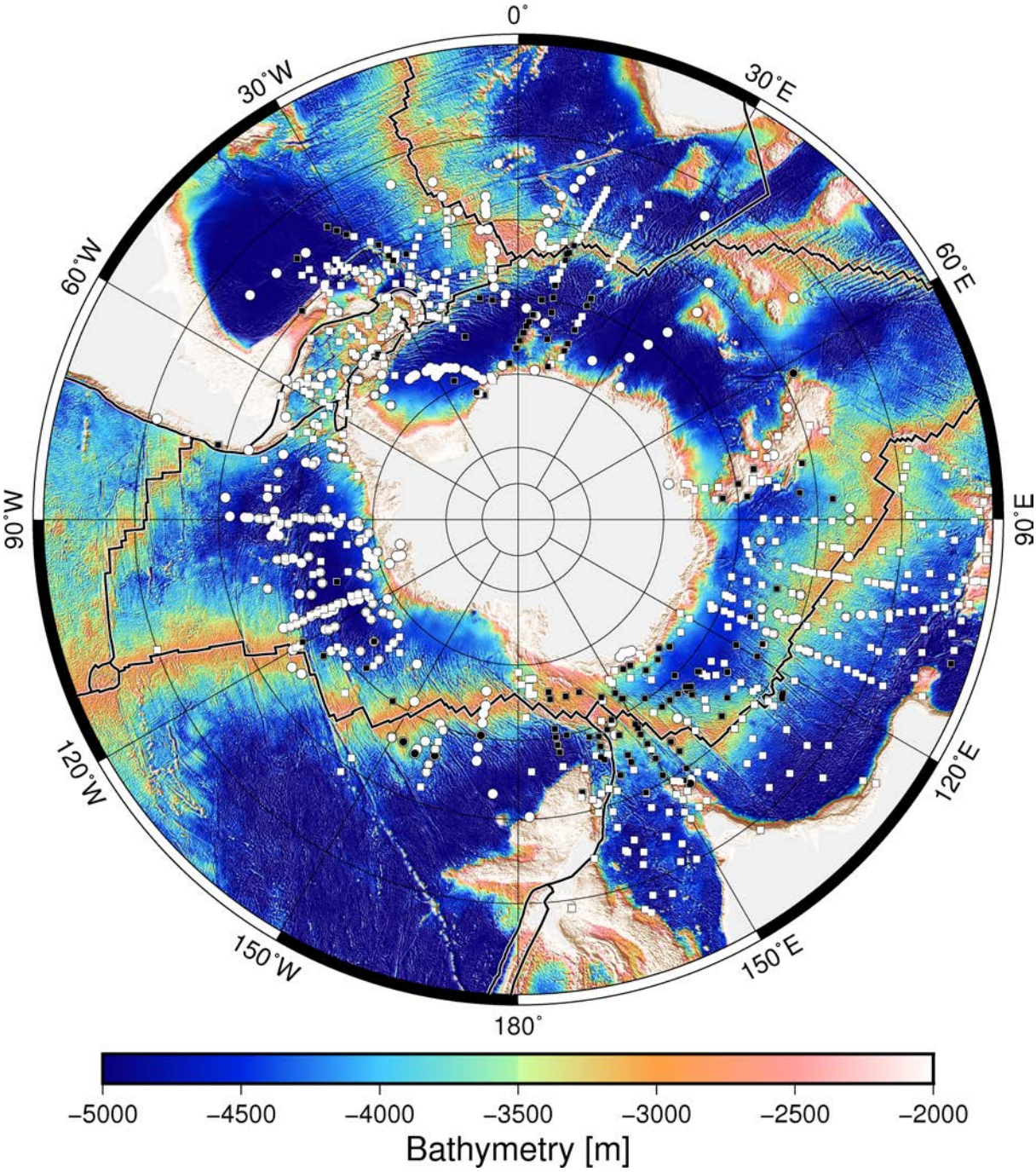


**Figure DR8.** Bathymetry overlain by conformities (white squares and white circles) and unconformities (black squares and black circles) in surface sediment of Bruhnes age. See caption in Fig. DR7 for detail. Black lines with white outlines denote plate boundaries. Bathymetry is from the ETOPO1 E 1 Arc-Minute Global Relief Model (Amante and Eakins, 2009). Stereographic projection.

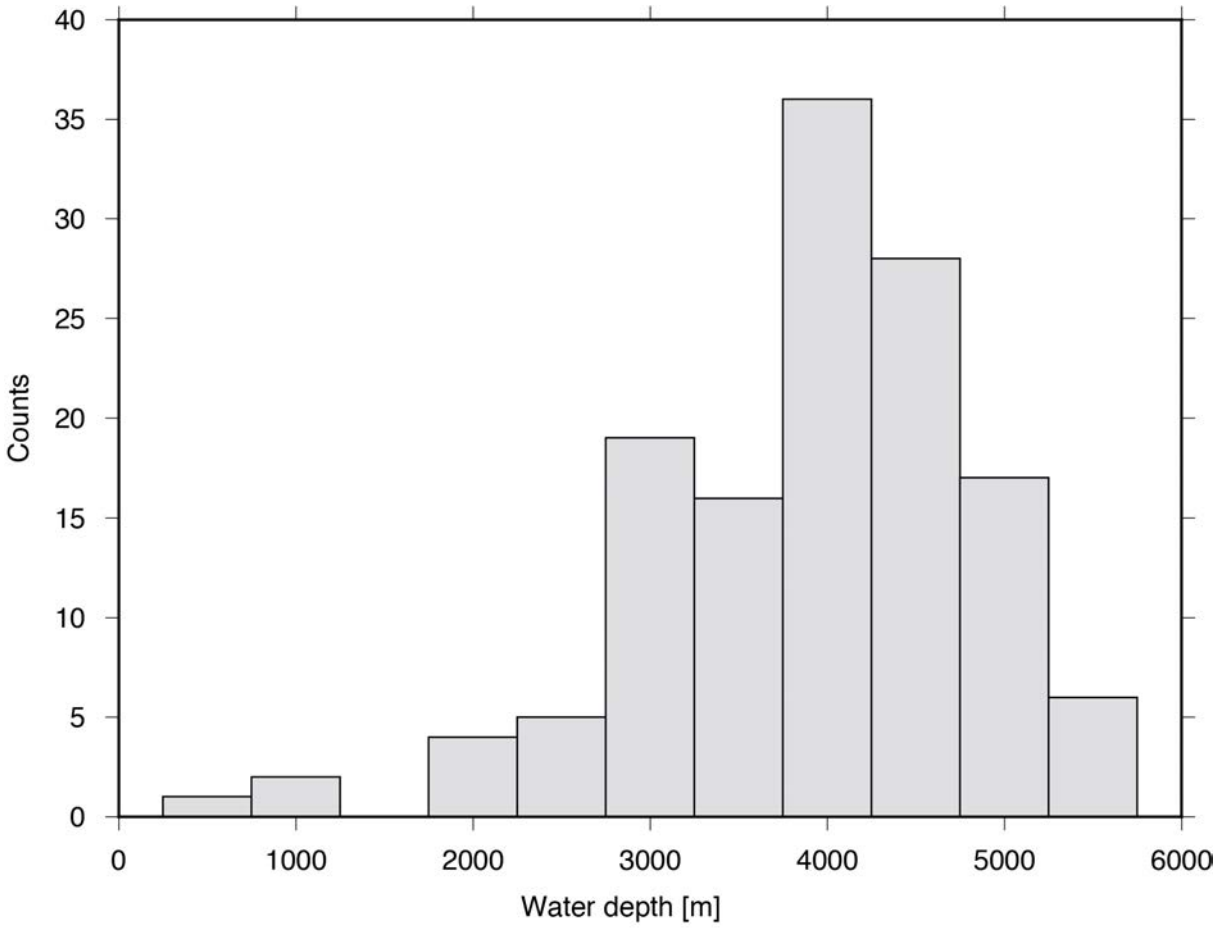


**Figure DR9.** Frequency of Brunhes age unconformity occurrence versus depth for the Southern Ocean. See caption for Figure DR7 for detail.

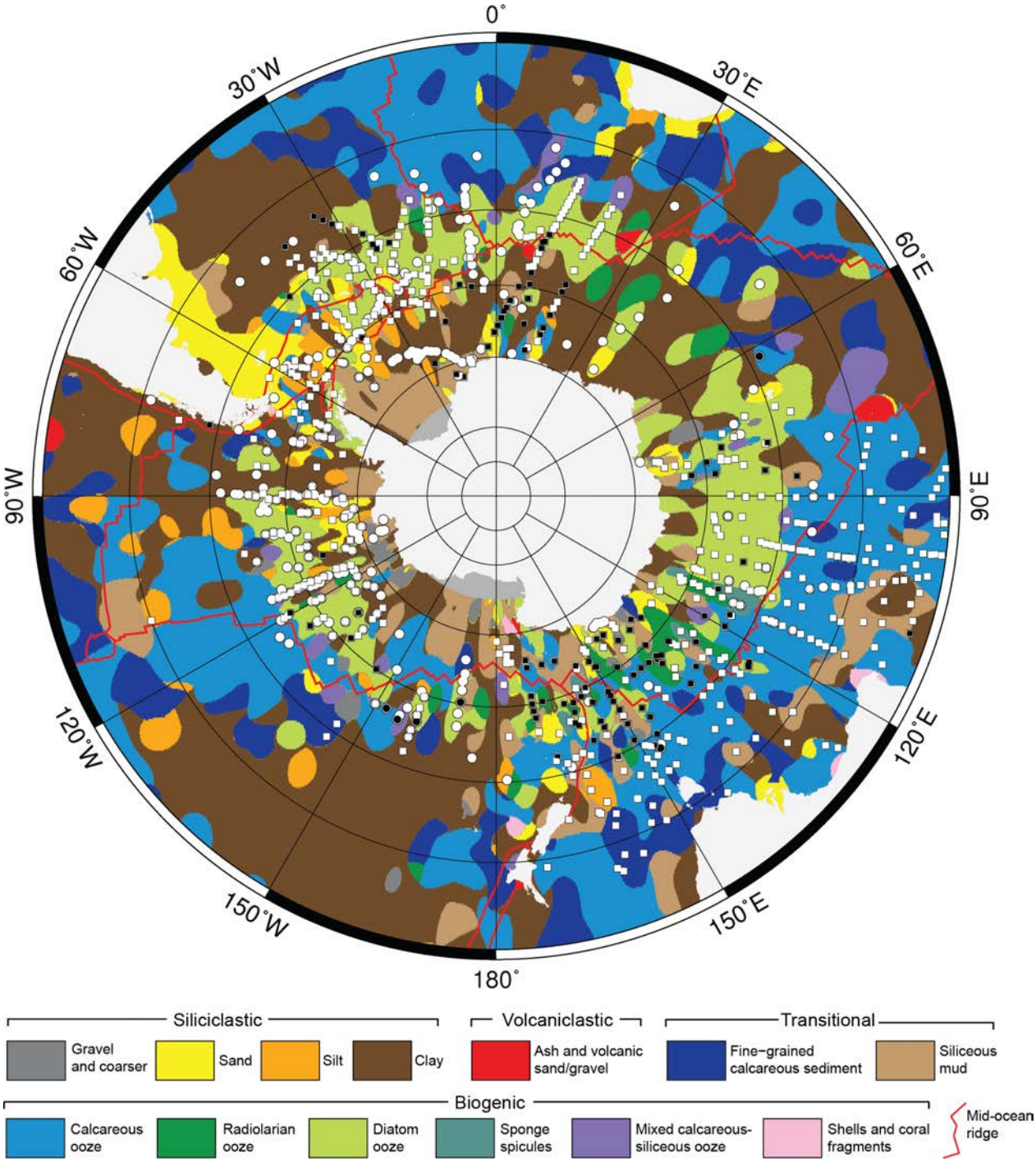


**Figure DR10.** Seafloor lithologies from Dutkiewicz et al. (2015) overlain by conformities (white squares and white circles) and unconformities (black squares and black circles) in surface sediment of Bruhnes age (see Fig. DR7 caption for detail). Stereographic projection.

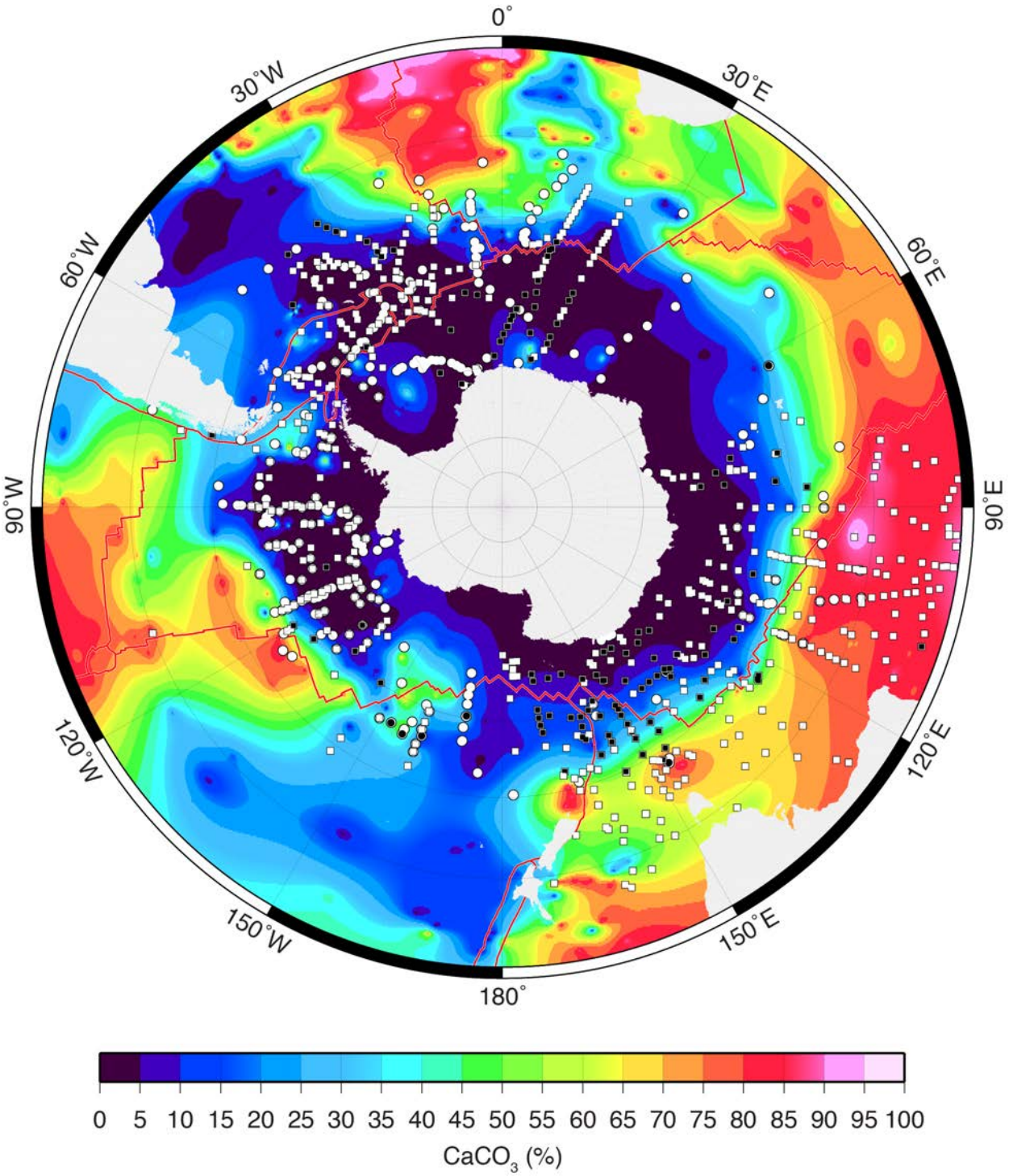


**Figure DR11.** Gridded map of $CaCO_3$ concentrations in surface sediments using combined data from Archer (1999), Bohrmann (1999) and Chase and Burckle (2015) overlain by conformities (white squares and white circles) and unconformities (black squares and black circles) in surface sediment of Bruhnes age (see Fig. DR7 caption for detail). Red lines denote plate boundaries. Gridding was done using an anisotropic spline with tension of 0.5. Stereographic projection.

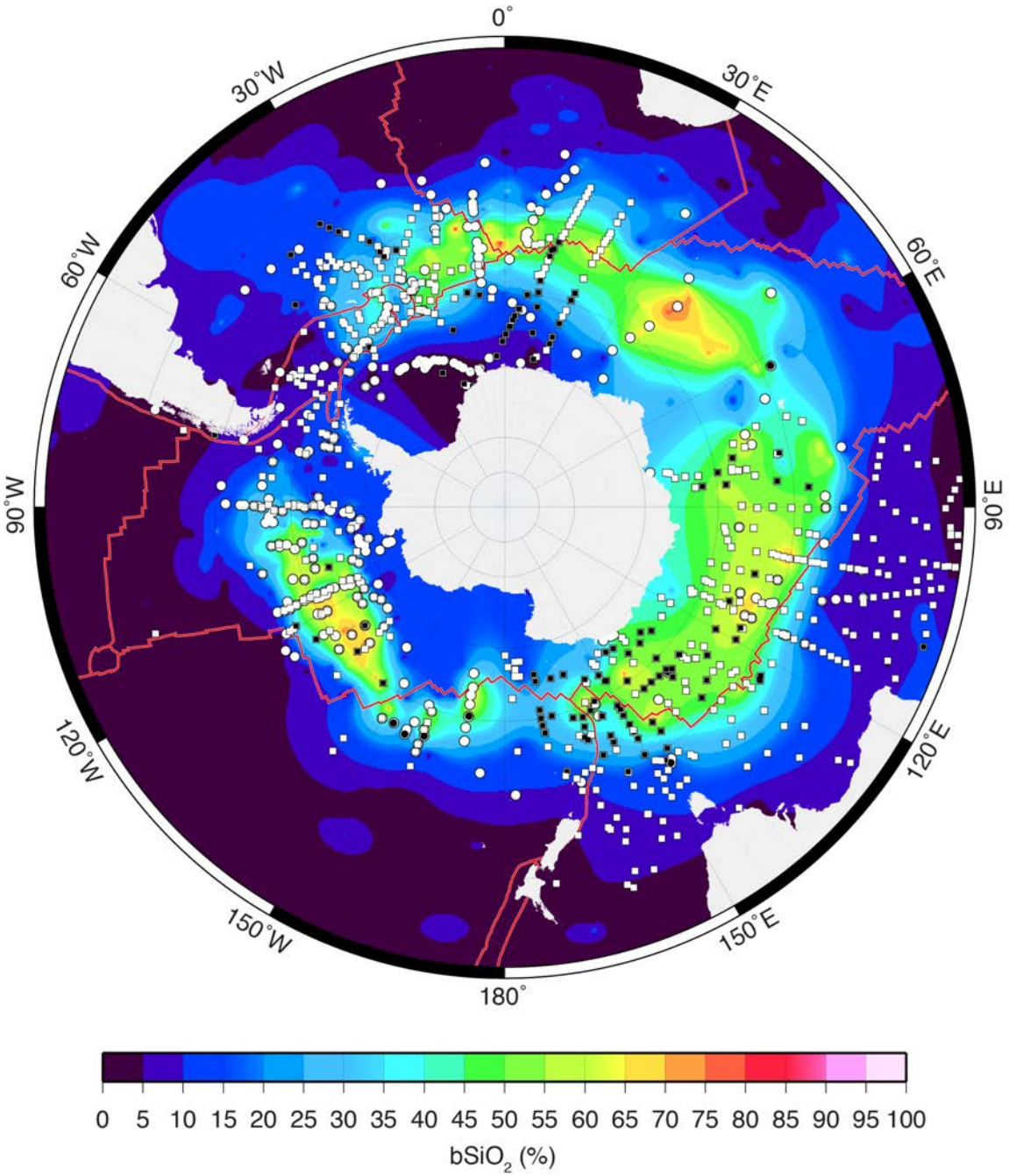


**Figure DR12.** Gridded map of $bSiO_2$ concentrations in surface sediments using combined data from Archer (1999), Bohrmann (1999) and Chase and Burckle (2015) overlain by conformities (white squares and white circles) and unconformities (black squares and black circles) in surface sediment of Bruhnes age (see Fig. DR7 caption for detail). Red lines denote plate boundaries. Gridding was done using an anisotropic spline with tension of 0.5. Stereographic projection.

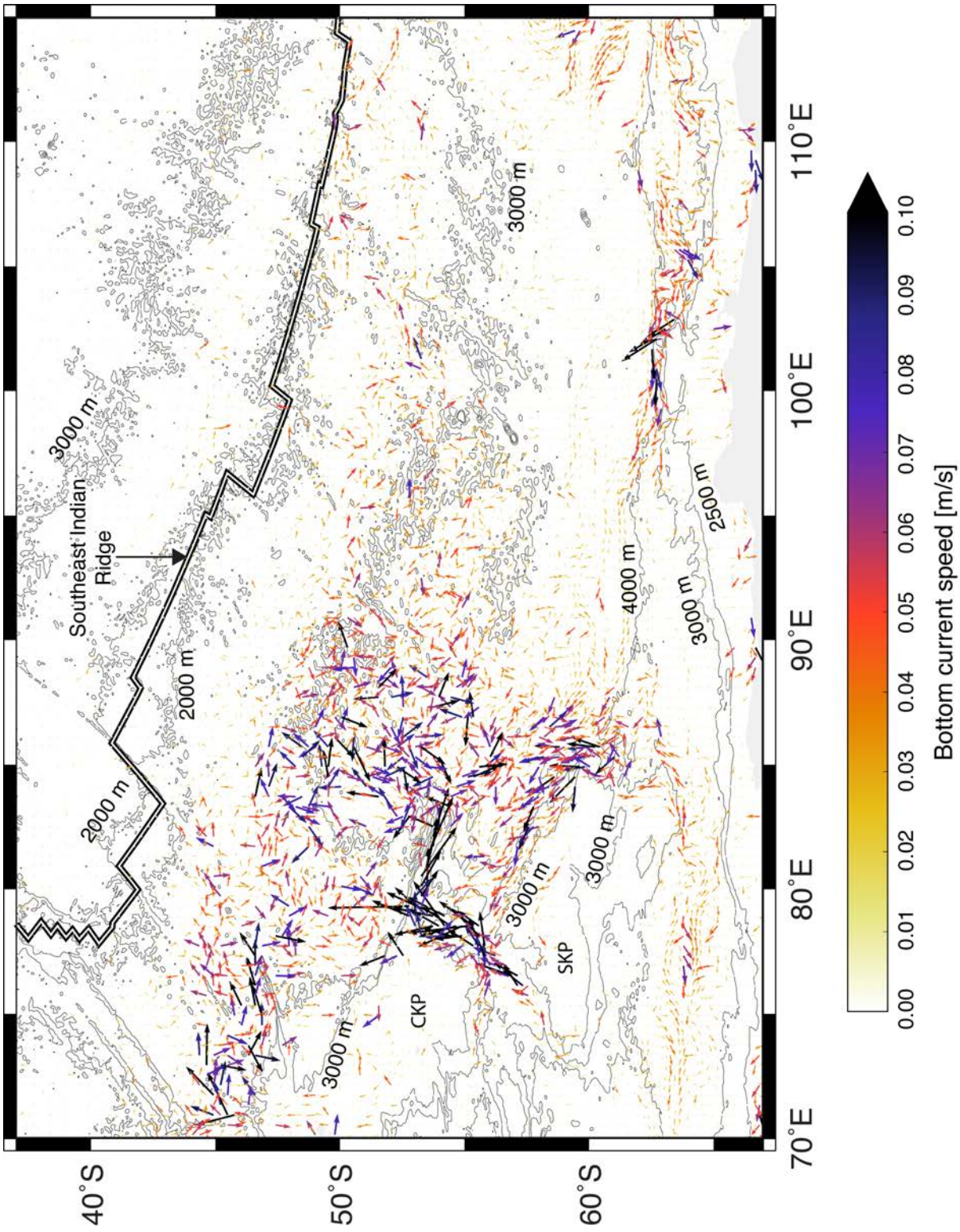


**Figure DR13.** Quiver plot overlying bathymetry contours for the western sector of the Southeast Indian Ridge. CKP – Central Kerguelen Plateau, SKP – Southern Kerguelen Plateau. Equidistant cylindrical projection.

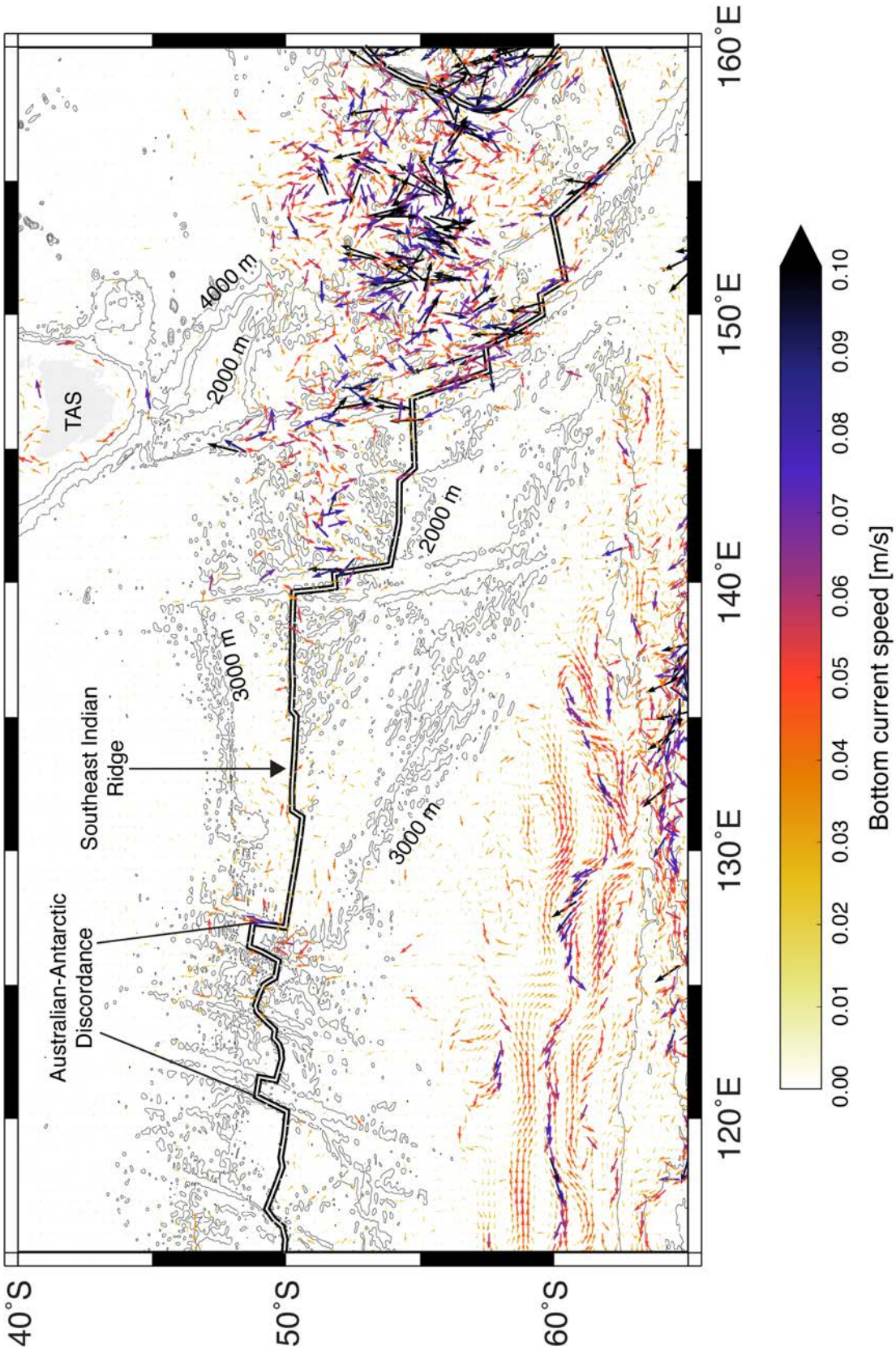


**Figure DR14.** Quiver plot overlying bathymetry contours for the eastern sector of the Southeast Indian Ridge. Equidistant cylindrical projection.

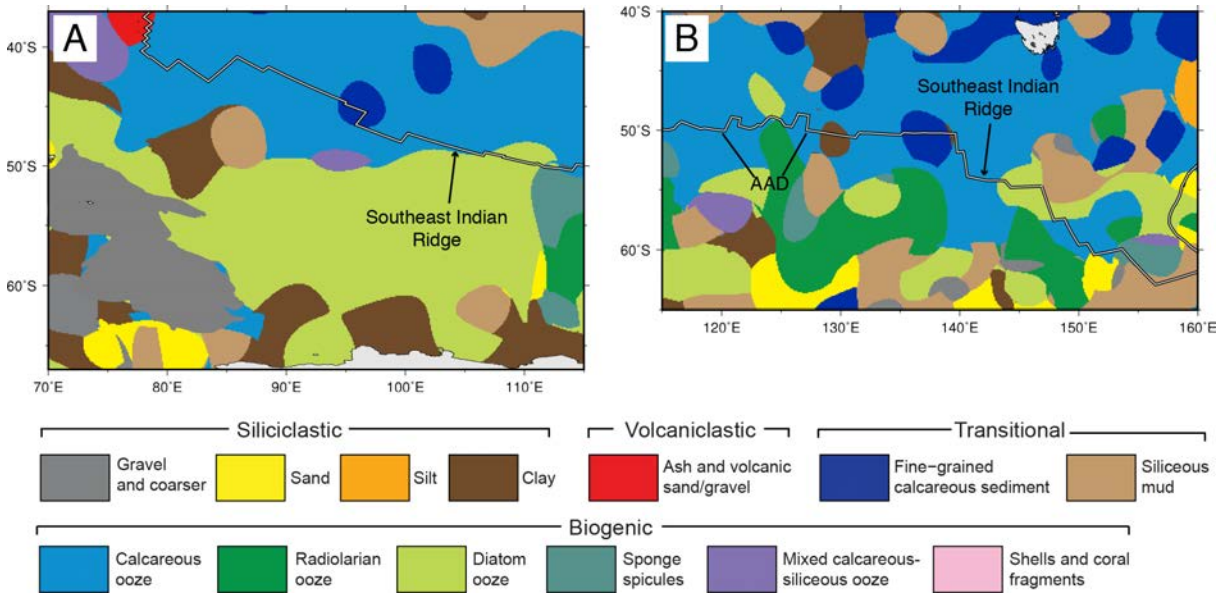


**Figure DR15.** Seafloor lithology from Dutkiewicz (2015) for the Southeast Indian Ridge region of the Southern Ocean. Equidistant cylindrical projection.

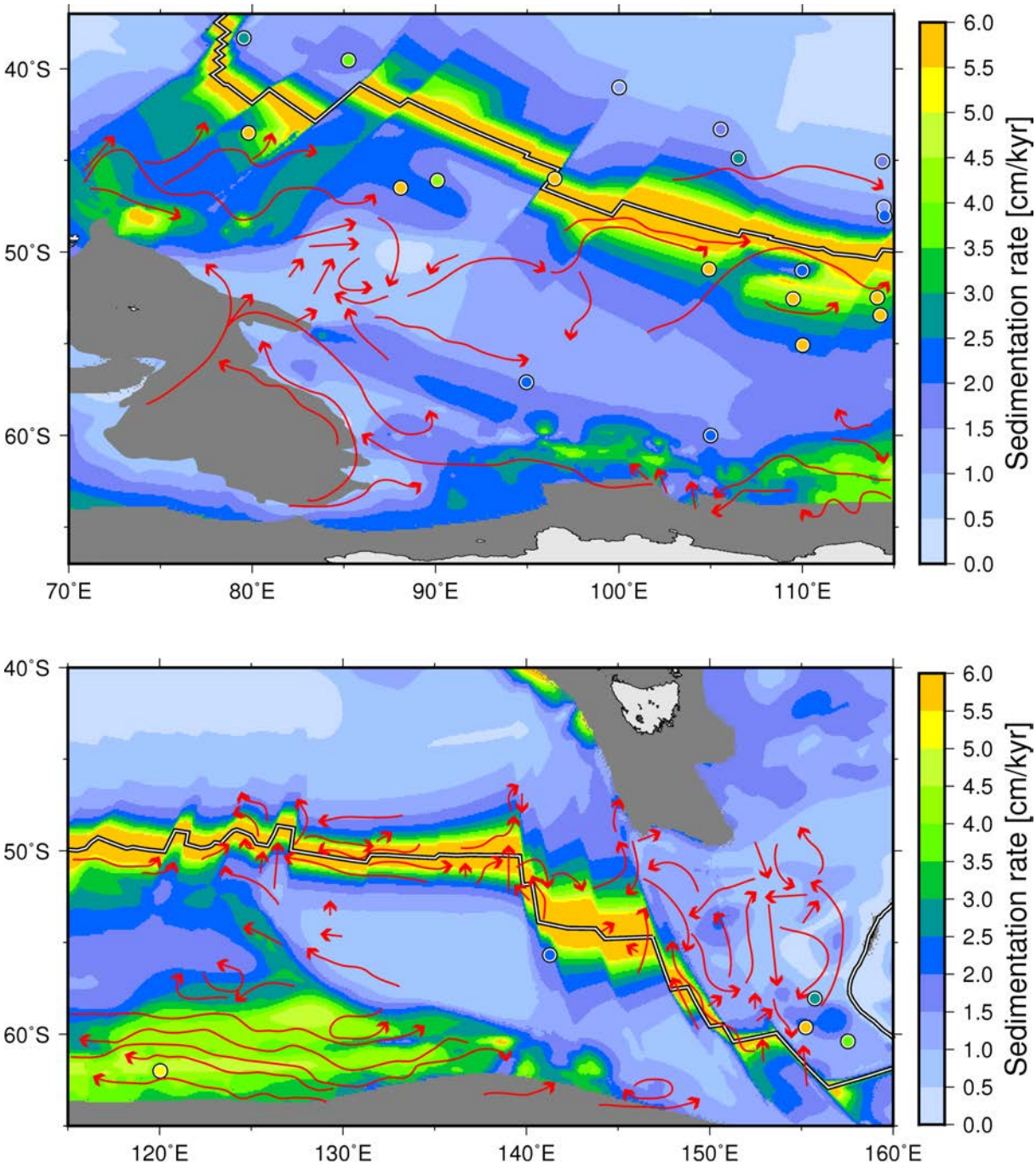


**Figure DR16.** Long-term average sedimentation rates in the Southern Ocean overlain with Holocene age-model derived sedimentation rates. Excess deposition of recent sediments along a mid-ocean ridge is expressed as bands of anomalously high sedimentation rates when computed by dividing the total sediment thickness by crustal age, with rates decreasing away from the mid-ocean ridge crest as the age of the crust increases. Black-white lines indicate plate boundaries. Red arrows indicate generalized bottom current directions based on quiver plots in Figs DR13 and 14. Equidistant cylindrical projection.

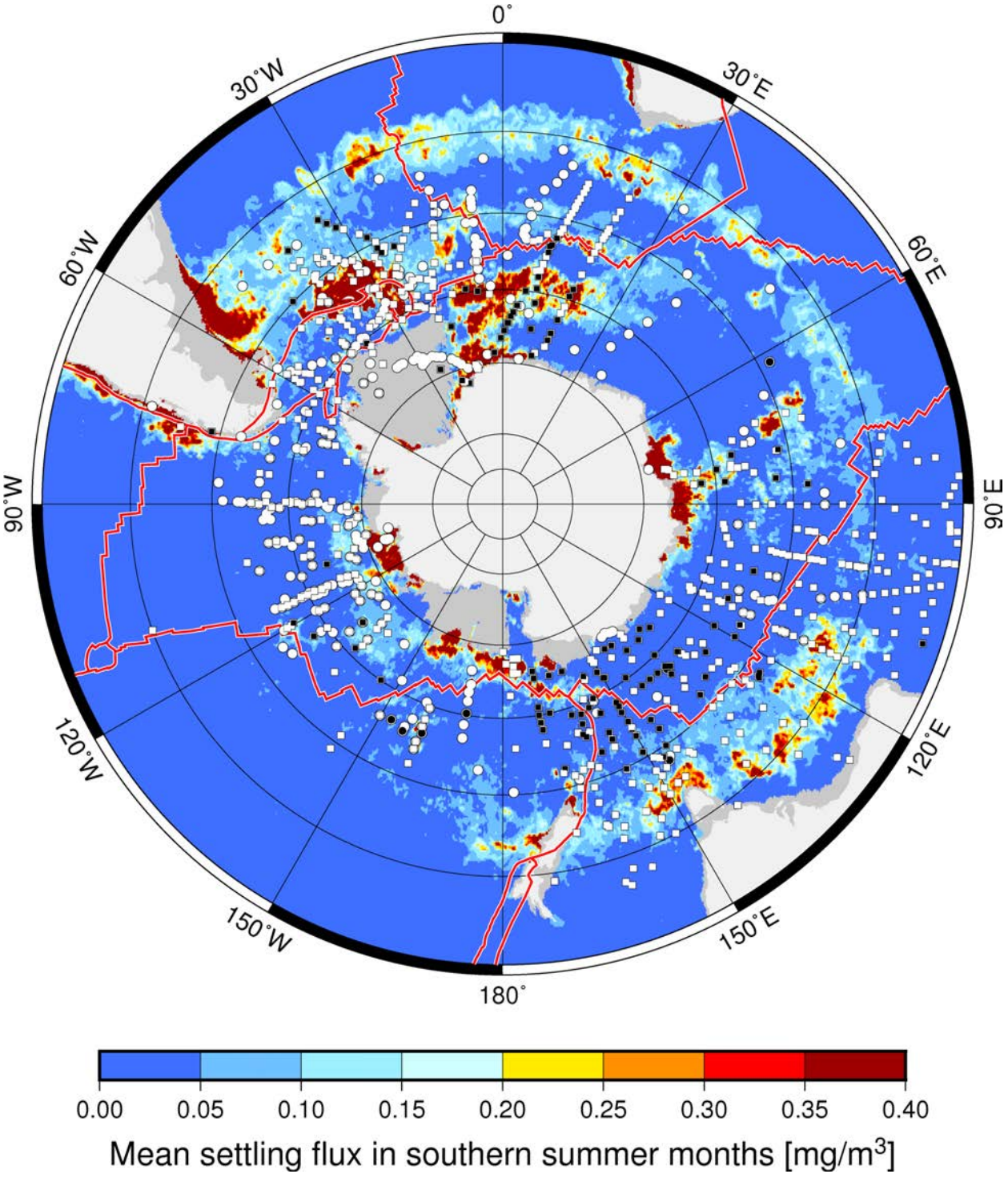


**Figure DR17.** Austral summer average of diatom chlorophyll concentrations for the period 2003-2013 (Soppa et al., 2014) overlain by conformities (white squares and white circles) and unconformities (black squares and black circles) in surface sediment of Bruhnes age (see Fig. DR7 caption for detail). Red lines with white outlines denote plate boundaries. Stereographic projection.

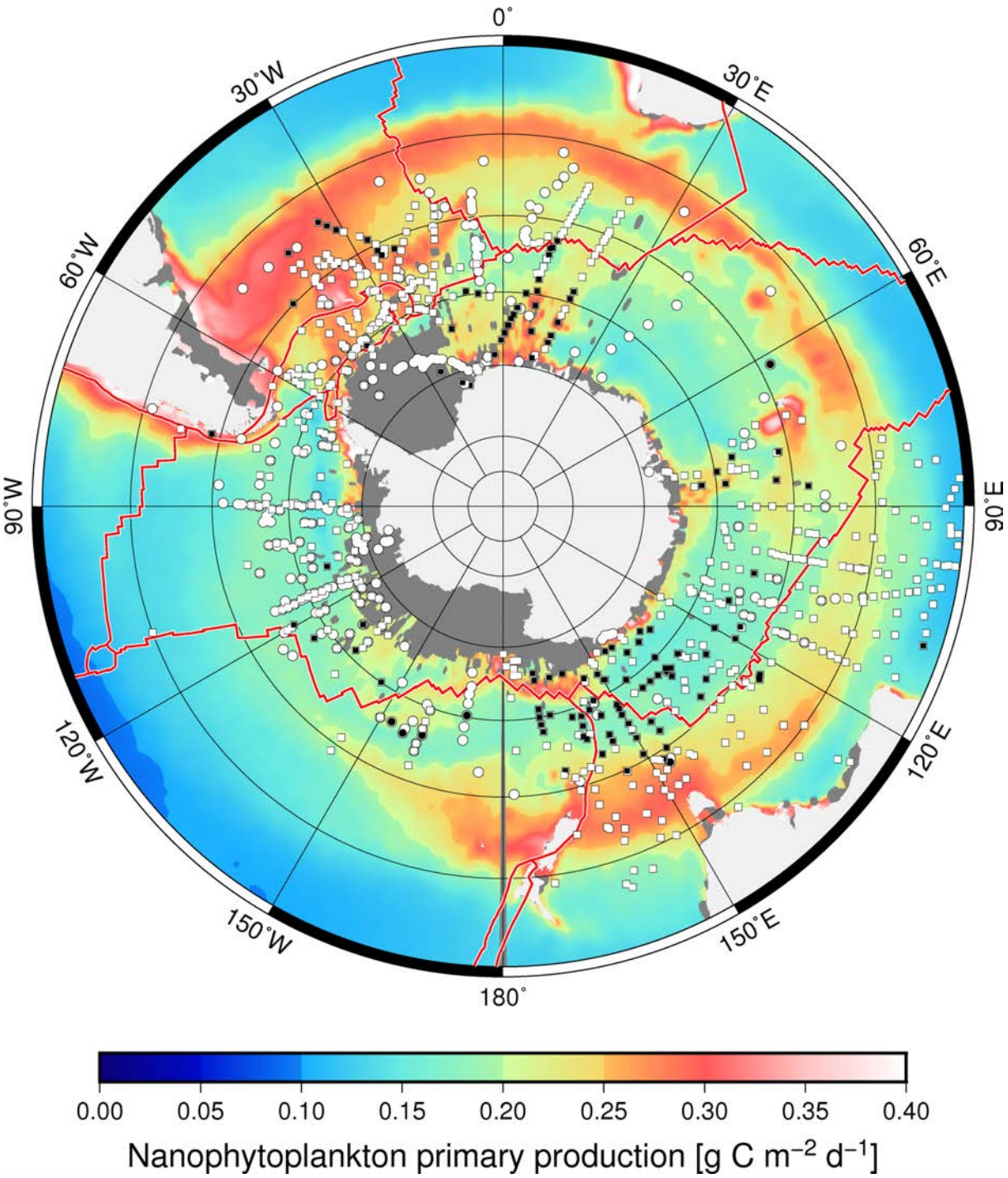


**Figure DR18.** Austral summer average of nanophytoplankon primary production for the period 1998-2007 (Uitz et al., 2010) overlain by conformities (white squares and white circles) and unconformities (black squares and black circles) in surface sediment of Bruhnes age (see Fig. DR7 caption for detail). Red lines with white outlines denote plate boundaries. Stereographic projection.

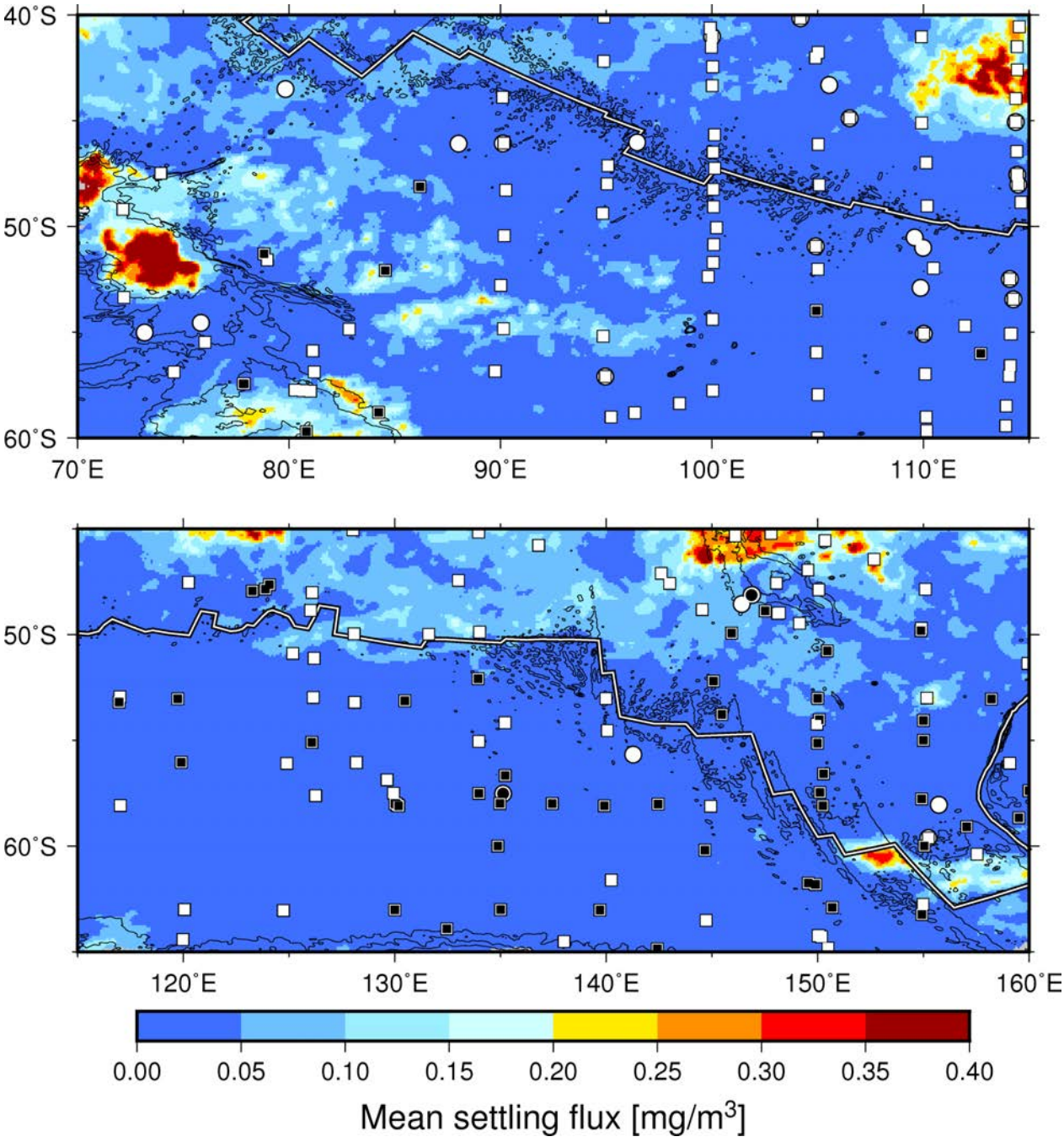


**Figure DR19.** Austral summer average of diatom chlorophyll concentrations for the period 2003-2013 (Soppa et al., 2014) overlain by conformities (white squares and white circles) and unconformities (black squares and black circles) in surface sediment of Bruhnes age (see Fig. DR7 caption for detail). Black-white lines denote plate boundaries. Equidistant cylindrical projection.

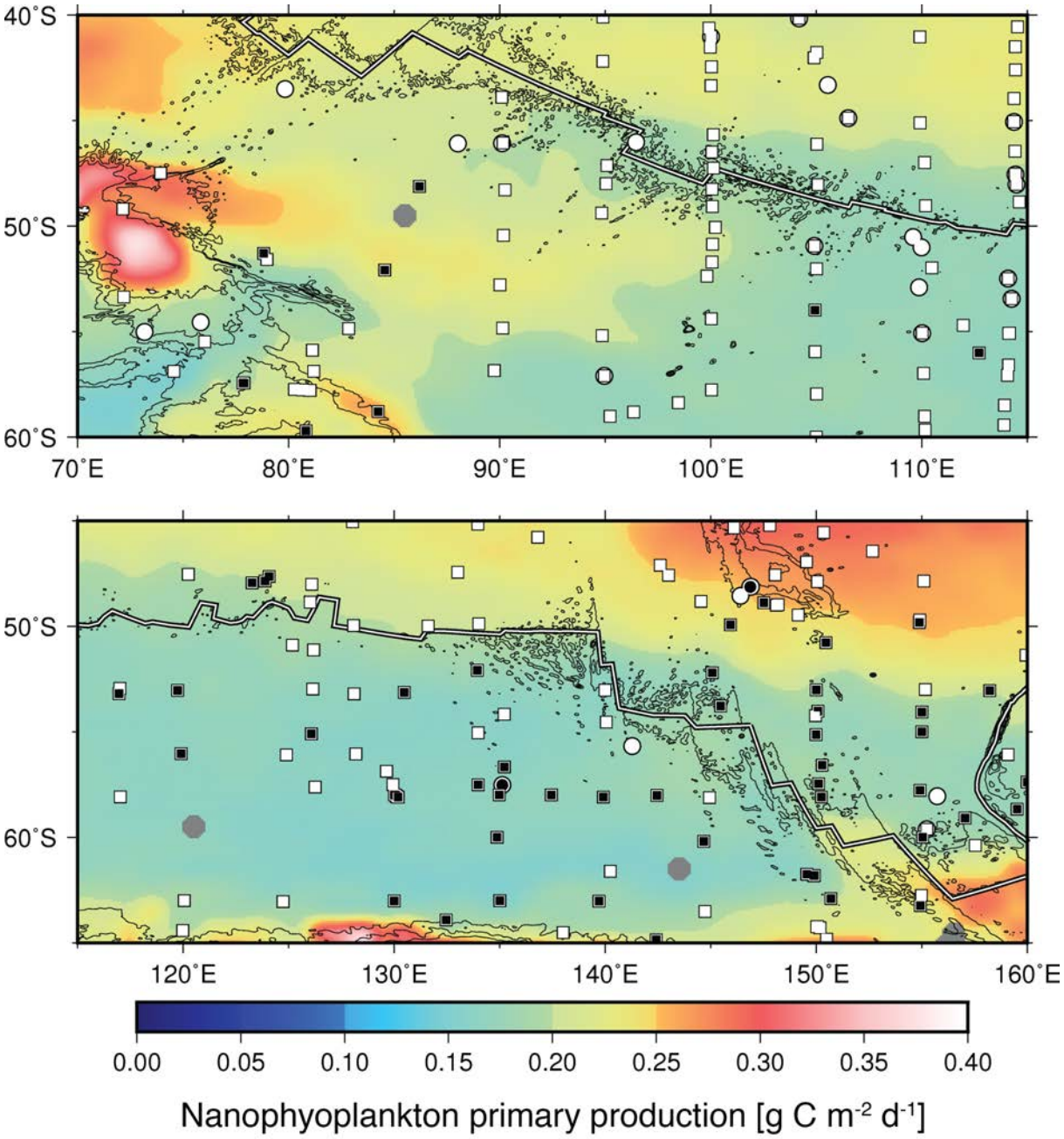


**Figure DR20.** Austral summer average of nanophytoplankon primary production for the period 1998-2007 (Uitz et al., 2010) overlain by conformities (white squares and white circles) and unconformities (black squares and black circles) in surface sediment of Bruhnes age (see Fig. DR7 caption for detail). Red lines denote mid-ocean ridges. Gray circles are artefacts in the productivity grid. Black-white lines indicate plate boundaries. Equidistant cylindrical projection.

**References:**


Allen, C. S., Pike, J., Pudsey, C. J., and Leventer, A., 2005a, Submillennial variations in ocean conditions during deglaciation based on diatom assemblages from the southwest Atlantic: Paleoceanography, v. 20, no. 2, p. PA2012,

-, 2005b, (Table 1) Age determination of sediment core KC073, 10.1594/PANGAEA.837085.

Amante, C., and Eakins, B. W., 2009, ETOPO1 1 Arc-Minute Global Relief Model: Procedures, Data Sources and Analysis, National Geophysical Data Center, NOAA, NOAA Technical Memorandum NESDIS NGDC-24, NOAA Technical Memorandum NESDIS NGDC-24.

Archer, D. E., 1996, An atlas of the distribution of calcium carbonate in sediments of the deep sea: Global Biogeochemical Cycles, v. 10, no. 1, p. 159-174,

Archer, D. E., 1999, Opal, quartz and calcium carbonate content in surface sediments of the ocean floor, 10.1594/PANGAEA.56017.

Bianchi, C., and Gersonde, R., 2004a, (Appendix Table 1) Age determination of sediment core PS1654-2, 10.1594/PANGAEA.712951.

Bianchi, C., and Gersonde, R., 2004b, (Appendix Table 1) Age determination of sediment core PS2090-1, 10.1594/PANGAEA.712952.

Bianchi, C., and Gersonde, R., 2004c, Climate evolution at the last deglaciation: the role of the Southern Ocean: Earth and Planetary Science Letters, v. 228, no. 3, p. 407-424,

Bohrmann, G., 1999, Geochemistry of surface sediments from the South Atlantic, 10.1594/PANGAEA.54956.

Bonn, W. J., Gingele, F. X., Grobe, H., Mackensen, A., and Fütterer, D. K., 1998a, Age model of sediment core PS1575-1, 10.1594/PANGAEA.50562.

-, 1998b, Age model of sediment core PS1821-6, 10.1594/PANGAEA.351294.

-, 1998c, Age model of sediment core PS2038-2, 10.1594/PANGAEA.351295.

-, 1998d, Palaeoproductivity at the Antarctic continental margin: opal and barium records for the last 400 ka: Palaeogeography, Palaeoclimatology, Palaeoecology, v. 139, no. 3, p. 195-211,

Bradtmiller, L. I., Anderson, R. F., Fleisher, M. Q., and Burckle, L. H., 2009, Comparing glacial and Holocene opal fluxes in the Pacific sector of the Southern Ocean: Paleoceanography, v. 24, no. 2,

Charles, C. D., and Fairbanks, R. G., 1992a, Evidence from Southern Ocean sediments for the effect of North Atlantic deep-water flux on climate: Nature, v. 355, p. 416-419,

Charles, C. D., and Fairbanks, R. G., 1992b, (Table 1) Age determination of sediment core RC11-83., 10.1594/PANGAEA.726261.

Chase, Z., Anderson, R. F., Fleisher, M. Q., and Kubik, P. W., 2003, Accumulation of biogenic and lithogenic material in the Pacific sector of the Southern Ocean during the past 40,000 years: Deep Sea Research Part II: Topical Studies in Oceanography, v. 50, no. 3, p. 799-832, doi:10.1016/S0967-0645(02)00595-7.

Chase, Z., and Burckle, L. H., 2015, Compilation of $^{230}$Th-normalized opal burial and opal concentrations from Southern Ocean surface sediments, 10.1594/PANGAEA.846117.

Chase, Z., Kohfeld, K. E., and Matsumoto, K., 2015, Controls on biogenic silica burial in the Southern Ocean: Global Biogeochemical Cycles, v. 29, no. 10, p. 1599-1616, doi: 10.1002/2015GB005186.

Dezileau, L., Bareille, G., Reyss, J. L., and Lemoine, F., 2000, Evidence for strong sediment redistribution by bottom currents along the southeast Indian ridge: Deep Sea Research Part I: Oceanographic Research Papers, v. 47, no. 10, p. 1899-1936, doi:10.1016/S0967-0637(00)00008-X.
Divins, D. L., 2004, Total Sediment Thickness of the World's Oceans and Marginal Seas,
Domack, E. W., Jull, A. J. T., and Nakao, S., 1991a, Advance of East Antarctic outlet glaciers during the Hypsithermal: implications for the volume state of the Antarctic ice sheet under global warming: Geology, v. 19, no. 11, p. 1059-1062,
-, 1991b, (Table 1) Age determinations on ODP Hole 119-740A, 10.1594/PANGAEA.389054.
-, 1991c, (Table 1) Age determinations on sediment core Core302, 10.1594/PANGAEA.389055.
-, 1991d, (Table 1) Age determinations on sediment core DF79.009-GB, 10.1594/PANGAEA.389056.
-, 1991e, (Table 1) Age determinations on sediment core DF79.012-GB, 10.1594/PANGAEA.389057.
Dutkiewicz, A., Müller, R. D., O'Callaghan, S., and Jónasson, H., 2015, Census of seafloor sediments in the world's ocean: Geology, v. 43, no. 9, p. 795-798,
Francois, R., Bacon, M. P., Altabet, M. A., and Labeyrie, L. D., 1993, Glacial/interglacial changes in sediment rain rate in the SW Indian sector of Subantarctic waters as recorded by 230Th, 231Pa, U, and δ15N: Paleoceanography, v. 8, no. 5, p. 611-629,
Francois, R., Frank, M., Rutgers van der Loeff, M. M., and Bacon, M. P., 2004, $^{230}$Th normalization: An essential tool for interpreting sedimentary fluxes during the late Quaternary: Paleoceanography, v. 19, no. 1, p. 1-16,
Frank, M., 2002a, Age model of sediment core PS1754-1, doi:10.1594/PANGAEA.81109.
-, 2002b, Age model of sediment core PS1772-8, doi:10.1594/PANGAEA.81108.
Frank, M., Gersonde, R., and Mangini, A., 1999, Sediment redistribution, $^{230}Th_{ex}$-normalization and implications for the reconstruction of particle flux and export paleoproductivity, *in* Fischer, G., and Wefer, G., eds., Use of Proxies in Paleoceanography: Examples from the South Atlantic: Berlin Heidelberg, Springer-Verlag, p. 409-426.
Frank, M., and Mackensen, A., 2002a, Age model of sediment core PS1756-5, doi:10.1594/PANGAEA.81106.
Frank, M., and Mackensen, A., 2002b, Age model of sediment core PS2082-1, doi:10.1594/PANGAEA.81103.
Froelich, P. N., Malone, P. N., Hodell, D. A., Ciesielski, P. F., Warnke, D. A., Westall, F., Hailwood, E. A., Nobes, D. C., Fenner, J., and Mienert, J., Biogenic opal and carbonate accumulation rates in the subantarctic South Atlantic: the late Neogene of Meteor Rise Site 704, *in* Proceedings Proc. Ocean Drill. Program Sci. Results1991, Volume 114, p. 515-550.
Geibert, W., Rutgers van der Loeff, M. M., Usbeck, R., Gersonde, R., Kuhn, G., and Seeberg‐Elverfeldt, J., 2005, Quantifying the opal belt in the Atlantic and southeast Pacific sector of the Southern Ocean by means of $^{230}$Th normalization: Global Biogeochemical Cycles, v. 19, no. 4, p. 1-13, doi: 10.1029/2005GB002465.
Goodell, H. G., and Watkins, N. D., 1968, The paleomagnetic stratigraphy of the Southern Ocean: 20° West to 160° East longitude: Deep Sea Research and Oceanographic Abstracts, v. 15, p. 89-112, doi:10.1016/0011-7471(68)90030-2.

Gozhik, P. F., Orlovsky, G. N., Mitin, L. I., Pavlov, A. Y., Rud, L. M., Yanchuk, E. A., Ivanik, M. M., Vodopyan, N. S., and Krasnozhina, Z. V., 1991a, Geologiya i Metallogeniya Yuzhnogo Okeana (Geology and Metallogeny of the Southern Ocean), *in* Shnyukov, E. F., ed., Naukova Dumka (Kiev): in Russian, p. 192.
-, 1991b, (Table 13) Radiocarbon age of bottom sediments from the Southern Ocean, 10.1594/PANGAEA.782426.
Grobe, H., and Mackensen, A., 1992a, Age model of sediment core PS1380-3, 10.1594/PANGAEA.50558.
-, 1992b, Late Quaternary climatic cycles as recorded in sediments from the Antarctic continental margin, *in* Kennett, J. P., and Warnke, D. A., eds., The Antarctic Paleoenvironment: a perspective on Global Change, Antarctic Research Series, American Geophysical Union.
Howard, W. R., and Prell, W. L., 1994a, Age model of sediment core MD84-529., 10.1594/PANGAEA.263948.
-, 1994b, Age model of sediment core RC13-229, 10.1594/PANGAEA.52655.
Howard, W. R., and Prell, W. L., 1994c, Late Quaternary $CaCO_3$ production and preservation in the Southern Ocean: Implications for oceanic and atmospheric carbon cycling: Paleoceanography, v. 9, no. 3, p. 453-482,
Jacot Des Combes, H., Esper, O., De La Rocha, C. L., Abelmann, A., Gersonde, R., Yam, R., and Shemesh, A., 2008a, Diatom $\delta^{13}C$, $\delta^{15}N$, and C/N since the Last Glacial Maximum in the Southern Ocean: Potential impact of species composition: Paleoceanography, v. 23, no. 4, p. PA4209,
-, 2008b, (Table 1) Age determination of sediment cores from the Southern Ocean,
Kennett, J. P., and Watkins, N. D., 1976, Regional deep-sea dynamic processes recorded by late Cenozoic sediments of the southeastern Indian Ocean: Geological Society of America Bulletin, v. 87, no. 3, p. 321-339, doi: 10.1130/0016-7606(1976)87<321:RDDPRB>2.0.CO;2.
Kirshner, A. E., Anderson, J. B., Jakobsson, M., O'Regan, M., Majewski, W., and Nitsche, F. O., 2012a, Post-LGM deglaciation in Pine island Bay, west Antarctica: Quaternary Science Reviews, v. 38, p. 11-26,
-, 2012b, (Table 1) Radiocarbon ages of sediment cores obtained during Icebreaker Oden cruise OSO0910, Pine Island Bay, 10.1594/PANGAEA.812067.
Labeyrie, L., Labracherie, M., Gorfti, N., Pichon, J. J., Vautravers, M., Arnold, M., Duplessy, J. C., Paterne, M., Michel, E., and Duprat, J., 1996a, Hydrographic changes of the Southern Ocean (southeast Indian sector) over the last 230 kyr: Paleoceanography, v. 11, no. 1, p. 57-76,
-, 1996b, (Table 3) Age determination of sediment core MD88-770, 10.1594/PANGAEA.52730.
Labracherie, M., Labeyrie, L. D., Duprat, J., Bard, E., Arnold, M., Pichon, J.-J., and Duplessy, J.-C., (Table 4) Age determinations on sediment core MD84-527, 10.1594/PANGAEA.358352.
-, 1989a, Age determinations on sediment core MD73-025, 10.1594/PANGAEA.358348.
-, 1989b, (Table 4) Age determinations on sediment core MD84-551, 10.1594/PANGAEA.358353.
Labracherie, M., Labeyrie, L. D., Duprat, J., Bard, E., Arnold, M., Pichon, J. J., and Duplessy, J. C., 1989c, The last deglaciation in the Southern Ocean: Paleoceanography, v. 4, no. 6, p. 629-638,
Lamy, F., Arz, H. W., Kilian, R., Lange, C. B., Lembke-Jene, L., Wengler, M., Kaiser, J., Baeza-Urrea, O., Hall, I. R., and Harada, N., 2015a, Glacial reduction and millennial-scale

variations in Drake Passage throughflow: Proceedings of the National Academy of Sciences, v. 112, no. 44, p. 13496-13501,
-, 2015b, (Table S1) Age model of sediment core 202-1233, 10.1594/PANGAEA.848126.
-, 2015c, (Table S1) Age model of sediment core MD07-3128, 10.1594/PANGAEA.848127.
-, 2015d, (Table S1) Age model of sediment core MR0806-PC09, 10.1594/PANGAEA.848128.
Lamy, F., Gersonde, R., Winckler, G., Esper, O., Jaeschke, A., Kuhn, G., Ullermann, J., Martínez-Garcia, A., Lambert, F., and Kilian, R., 2014a, Age control points of sediment core PS75/056-1, 10.1594/PANGAEA.826579.
-, 2014b, Age control points of sediment core PS75/059-2, 10.1594/PANGAEA.826580.
-, 2014c, Age control points of sediment core PS75/074-3, 10.1594/PANGAEA.826581.
-, 2014d, Age control points of sediment core PS75/076-2, 10.1594/PANGAEA.826582.
-, 2014e, Age control points of sediment core PS75/079-2, 10.1594/PANGAEA.826583.
-, 2014f, Age control points of sediment core PS75/083-1, 10.1594/PANGAEA.826584.
-, 2014g, Increased dust deposition in the Pacific Southern Ocean during glacial periods: Science, v. 343, no. 6169, p. 403-407,
Ledbetter, M. T., and Ciesielski, P. F., 1986, Post-Miocene disconformities and paleoceanography in the Atlantic sector of the Southern Ocean: Palaeogeography, Palaeoclimatology, Palaeoecology, v. 52, no. 3, p. 185-214, doi:10.1016/0031-0182(86)90046-5.
Mackensen, A., 1996, Age model of sediment core PS1768-8, doi:10.1594/PANGAEA.50559.
Mackensen, A., Grobe, H., Hubberten, H.-W., and Kuhn, G., 1994a, Age model of sediment core PS1506-1, 10.1594/PANGAEA.50166.
-, 1994b, Age model of sediment core PS2082-1, 10.1594/PANGAEA.50167.
-, 1994c, Benthic foraminiferal assemblages and the d $\delta^{13}$C-signal in the atlantic sector of the Southern Ocean: glacial-to-interglacial contrasts, *in* Zahn, R., Pederson, T. F., Kaminiski, M. A., and Labeyrie, L., eds., Carbon Cycling in the Glacial Ocean: Constraints on the Ocean's Role in Global Change, Volume NATO ASI Series I17: Berlin, Heidelberg, Springer-Verlag, p. 105-144.
Mackensen, A., Rudolph, M., and Kuhn, G., 2001a, Age model of sediment core PS2498-1, doi:10.1594/PANGAEA.80801.
-, 2001b, (Table 2c) Age, TOC, primary production, and isotopes (Cibicidoides spp.) of sediment core PS2499-5, doi:10.1594/PANGAEA.65927.
Maddison, E. J., Pike, J., and Dunbar, R., 2012a, Seasonally laminated diatom-rich sediments from Dumont d'Urville Trough, East Antarctic Margin: Late-Holocene Neoglacial sea-ice conditions: The Holocene, v. 22, no. 8, p. 857-875,
-, 2012b, (Table 1) Radiocarbon ages for sediment cores MD03-2597, NBP01-01-JPC17B and NBP01-01-KC17B, 10.1177/0959683611434223.
Müller, R. D., Seton, M., Zahirovic, S., Williams, S. E., Matthews, K. J., Wright, N. M., Shephard, G. E., Maloney, K. T., Barnett-Moore, N., Hosseinpour, M., Bower, D. J., and Cannon, J., 2016, Ocean basin evolution and global-scale plate reorganization events since Pangea breakup: Annual Review of Earth and Planetary Sciences, v. 44, p. 107–138, 10.1146/annurev-earth-060115-012211.
Murayama, M., Nakamura, T., and Taira, A., 2000a, (Table 2) Age determination of sediment cores from the Tasman Plateau, 10.1594/PANGAEA.855345.

-, 2000b, Variations of terrestrial input and marine productivity in the Southern Ocean (48ºS) during the last two deglaciations: Paleoceanography, v. 15, no. 2, p. 170-180,
Osborn, N. I., Ciesielski, P. F., and Ledbetter, M. T., 1983, Disconformities and paleoceanography in the southeast Indian Ocean during the past 5.4 million years: Geological Society of America Bulletin, v. 94, no. 11, p. 1345-1358, doi: 10.1130/0016-7606(1983)94<1345:DAPITS>2.0.CO;2
Rebesco, M., Hernández-Molina, F. J., Van Rooij, D., and Wåhlin, A., 2014, Contourites and associated sediments controlled by deep-water circulation processes: state-of-the-art and future considerations: Marine Geology, v. 352, p. 111-154, doi:10.1016/j.margeo.2014.03.011.
Rosenthal, Y., Boyle, E. A., Labeyrie, L., and Oppo, D., 1995a, Glacial enrichments of authigenic Cd and U in Subantarctic sediments: A climatic control on the elements' oceanic budget?: Paleoceanography, v. 10, no. 3, p. 395-413,
-, 1995b, (Table 3) Sedimentation rate versus age in core MD80-304, 10.1594/PANGAEA.388560.
-, 1995c, (Table 3) Sedimentation rate versus age in core MD88-769., 10.1594/PANGAEA.388561.
-, 1995d, (Table 3) Sedimentation rate versus age in core RC13-229, 10.1594/PANGAEA.388562.
Shemesh, A., Hodell, D., Crosta, X., Kanfoush, S., Charles, C., and Guilderson, T., 2002a, Age-depth relation in sediment core TTN057-13-PC4, 10.1594/PANGAEA.842939.
-, 2002b, Sequence of events during the last deglaciation in Southern Ocean sediments and Antarctic ice cores: Paleoceanography, v. 17, no. 4, p. 8-1–8-7
Skinner, L. C., Fallon, S., Waelbroeck, C., Michel, E., and Barker, S., 2010a, (Table S1) Age determination of sediment core MD07-3076, planktonic foraminifera., 10.1594/PANGAEA.829756.
-, 2010b, Ventilation of the deep Southern Ocean and deglacial $CO_2$ rise: Science, v. 328, no. 5982, p. 1147-1151,
Soppa, M. A., Hirata, T., Silva, B., Dinter, T., Peeken, I., Wiegmann, S., and Bracher, A., 2014, Global retrieval of diatom abundance based on phytoplankton pigments and satellite data: Remote Sensing, v. 6, no. 10, p. 10,089-010,106, doi: 10.3390/rs61010089.
Suman, D. O., and Bacon, M. P., 1989, Variations in Holocene sedimentation in the North American Basin determined from $^{230}$Th measurements: Deep Sea Research Part A. Oceanographic Research Papers, v. 36, no. 6, p. 869-878, 10.1016/0198-0149(89)90033-2.
Uitz, J., Claustre, H., Gentili, B., and Stramski, D., 2010, Phytoplankton class‐specific primary production in the world's oceans: seasonal and interannual variability from satellite observations: Global Biogeochemical Cycles, v. 24, no. 3, 10.1029/2009GB003680.
Watkins, N. D., and Kennett, J. P., 1972, Regional sedimentary disconformities and Upper Cenozoic changes in bottom water velocities between Australasia and Antarctica: Antarctica Oceanology II: The Australian-New Zealand Sector, p. 273-293, doi: 10.1029/AR019p0273.
Yu, E.-F., 1994, Variations in the Particulate Flux of $^{230}$Th and $^{231}$Pa and Paleoceanographic Applications of the $^{231}$Pa/$^{230}$Th Ratio: Massachusetts Institute of Technology, 269 p.